NASA CONTRACTOR REPORT

STEADY SUBSONIC FLOW AROUND FINITE-THICKNESS WINGS

Ching-Chiang Kuo and Luigi Morino

Prepared by
BOSTON UNIVERSITY
Boston, Mass. 02215
for Langley Research Center

NATIONAL AERONAUTICS AND SPACE ADMINISTRATION • WASHINGTON, D. C. • NOVEMBER 1975

1. Report No.	2. Government Accession No.	3. Recipient's Catalog No.
NASA CR-2616		

4. Title and Subtitle	5. Report Date
STEADY SUBSONIC FLOW AROUND FINITE-THICKNESS WINGS	November 1975
	6. Performing Organization Code

7. Author(s)	8. Performing Organization Report No.
CHING-CHIANG KUO and LUIGI MORINO	TR-73-02
	10. Work Unit No.

9. Performing Organization Name and Address	11. Contract or Grant No.
DEPARTMENT OF AEROSPACE ENGINEERING BOSTON UNIVERSITY BOSTON, MASS. 02215	NGR 22-004-030

12. Sponsoring Agency Name and Address	13. Type of Report and Period Covered
	CONTRACTOR REPORT
	14. Sponsoring Agency Code

15. Supplementary Notes

THIS REPORT CONTAINS FURTHER DEVELOPMENT AND APPLICATION OF THE GENERAL METHOD DERIVED IN NASA CR-2464 (BOSTON UNIVERSITY REPORT TR-73-01). Dr. E. Carson Yates, Jr. of NASA Langley Research Center acted as technical advisor. Topical report.

16. Abstract

THE GENERAL METHOD FOR ANALYZING STEADY SUBSONIC POTENTIAL AERODYNAMIC FLOW AROUND A LIFTING BODY HAVING ARBITRARY SHAPE IS PRESENTED. BY USING THE GREEN FUNCTION METHOD, AN INTEGRAL REPRESENTATION FOR THE POTENTIAL IS OBTAINED. UNDER SMALL PERTURBATION ASSUMPTION, THE POTENTIAL AT ANY POINT, P, IN THE FIELD DEPENDS ONLY UPON THE VALUES OF THE POTENTIAL AND ITS NORMAL DERIVATIVE ON THE SURFACE, Σ_s, OF THE BODY. HENCE IF THE POINT P APPROACHES THE SURFACE OF THE BODY, THE REPRESENTATION REDUCES TO AN INTEGRAL EQUATION RELATING THE POTENTIAL AND ITS NORMAL DERIVATIVE (WHICH IS KNOWN FROM THE BOUNDARY CONDITIONS) ON THE SURFACE Σ_s (TWO-DIMENSIONAL FREDHOLM INTEGRAL EQUATION OF SECOND-TYPE). THE QUESTION OF UNIQUENESS IS EXAMINED AND IT IS SHOWN THAT, FOR THIN WINGS, THE OPERATOR BECOMES SINGULAR AS THE THICKNESS APPROACHES ZERO. THIS FACT MAY YIELD NUMERICAL PROBLEMS FOR VERY THIN WINGS. HOWEVER, NUMERICAL RESULTS OBTAINED FOR A RECTANGULAR WING IN SUBSONIC FLOW SHOW THAT THESE PROBLEMS DO NOT APPEAR EVEN FOR THICKNESS RATIO $\tau = .001$. COMPARISON WITH EXISTING RESULTS SHOW THAT THE PROPOSED METHOD IS AT LEAST AS FAST AND ACCURATE AS THE LIFTING SURFACE THEORIES.

17. Key Words (Suggested by Author(s))	18. Distribution Statement
POTENTIAL FLOW LIFTING SURFACE THEORY UNSTEADY FLOW AIRCRAFT AERODYNAMICS	UNCLASSIFIED – UNLIMITED Subject Category 02

19. Security Classif. (of this report)	20. Security Classif. (of this page)	21. No. of Pages	22. Price*
UNCLASSIFIED	UNCLASSIFIED	89	$4.75

*For sale by the National Technical Information Service, Springfield, Virginia 22161

SUMMARY

The general method for analyzing steady subsonic potential aerodynamic flow around a lifting body having arbitrary shape is presented. By using the Green function method, an integral representation for the potential is obtained. Under small perturbation assumption, the potential at any point, P, in the field depends only upon the values of the potential and its normal derivative on the surface, Σ_B, of the body. Hence if the point P approaches the surface of the body, the representation reduces to an integral equation relating the potential and its normal derivative (which is known from the boundary conditions) on the surface Σ_B (two-dimensional Fredholm integral equation of second-type). The question of uniqueness is examined and it is shown that, for thin wings, the operator becomes singular as the thickness approaches zero. This fact may yield numerical problems for very thin wings. However, numerical results obtained for a rectangular wing in subsonic flow show that these problems do not appear even for thickness ratio $\tau = .001$. Comparison with existing results show that the proposed method is at least as fast and accurate as the lifting surface theories.

FOREWORD

The authors wish to thank their colleague P.T. Hsu for the discussion and comments as well as Mr. Emil Suciu for his help on the numerical calculations and Miss Beverly Wright for her patience in editing and typing this report.

CONTENTS

CONTENTS CONTINUED

LIST OF FIGURES

LIST OF SYMBOLS

a_∞	speed of sound in undisturbed air
a_{ki}	see Eq. 4.12
b	span of wing
b_k	see Eq. 4.6
c	chord of wing
c_p	pressure coefficient
$c_\ell = -\Delta c_p = c_{p,\ell} - c_{p,u}$	lifting pressure coefficient
c_{ki}	see Eq. 4.7
$\hat{c}_{ki}$	see Eq. 4.14
d_m, d_p	see Eq. B.2
E	domain function (Eq. 2.9 and Eq. A.1)
G	Green's function
h	thickness of wing
I_W	see Eq. 3.9
J_W	see Eq. 3.13
$M = v_\infty / a_\infty$	Mach number for undisturbed flow
$\vec{n}_1$	normal to the surface Σ at P_1
$N = 2 \cdot NX \cdot NY$	
NX, NY	number of boxes in direction X, Y
p	pressure
p_∞	pressure in undisturbed air
$P \equiv (X,Y,Z)$	control point
$P_1 \equiv (X_1, Y_1, Z_1)$	dummy point of integration on Σ
$P^{(k)}$	center of box Σ_k

P_*	control point on Σ
$r_\beta = \left\{(x - x_1)^2 + \beta^2 [(y - y_1)^2 + (z - z_1)^2]\right\}^{1/2}$	
$R = [(X - X_1)^2 + (Y - Y_1)^2 + (Z - Z_1)^2]^{1/2}$	
S	function describing the surface Σ
S_B	function describing the surface Σ_B
S_W	function describing the surface Σ_W
U_∞	velocity of undisturbed flow
w_{ki}	see Eqs. 4.9 and 4.10
x,y,z	Cartesian coordinate system in which the undisturbed air travels at velocity U_∞ in positive x direction
X,Y,Z	Prandtl-Glauert cartesian coordinate
$\bar{X},\bar{Y}$	see Eq. 4.27
X_c, Y_c	see Eq. 4.30
α	angle of attack (Eq. 7.5)
$\beta = \sqrt{1 - M^2}$	
γ	specific heat coefficient ratio
δ	Dirac's delta function
δ_{ki}	Kronecker delta
δ_ε	see Eq. A.4
$\Delta\bar{X}$, $\Delta\bar{Y}$	see Eq. 4.28
ε	radius of circular surface element Σ_ε
$\bar{\varepsilon}$	see Eq. 2.18
$\hat{\eta}_p$, $\hat{\eta}_m$	see Eq. B.15
$\hat{\xi}, \hat{\eta}, \hat{\zeta}$	see Eq. B.9
$\hat{\xi}_p$, $\hat{\xi}_m$	see Eqs. B.11 and B.12

$\hat{\xi}_{op}, \hat{\xi}_{om}, \hat{\xi}_{ip}, \hat{\xi}_{im}$	see Eq. B.13
ρ_∞	density of undisturbed air
Σ	surface surrounding body and wake
Σ_B	surface surrounding body
Σ_W	surface surrounding wake
Σ_w	surface of the wing
τ	thickness ratio
φ	perturbation aerodynamic potential
φ_k	value of φ at $P^{(k)}$
$\varphi_n = \partial\varphi/\partial n$	see Eq. 1.8
Φ	aerodynamic potential
Ω_n	solid angle for strip Σ'_n

SPECIAL SYMBOLS

∇	gradient operator in x,y,z coordinates
$\bar{\nabla}$	gradient operator in X,Y,Z coordinates
$\Delta( ) = ( )$ upper $-$ $( )$ lower	

SUBSCRIPTS

1	Dummy variables
TE	trailing edge
*	evaluation at $P = P_*$

SECTION 1

INTRODUCTION

A general method for compressible potential aerodynamics has been developed by one of the present authors*. Presented here are applications of the method to linearized steady subsonic flow. The method and the associated numerical procedure for evaluating surface pressure are described for general complex aircraft configurations. Numerical examples for finite-thickness wings are included.

1.1 Definition of Problem

The importance of an accurate evaluation of the flow field and related pressure distribution around an aircraft is well known to the aerospace designer. In the methods usually employed for the evaluation of the pressure distribution over a wing, the wing is assumed to have zero-thickness (lifting surface theories, see for instance Refs. 1 to 4). More recently more sophisticated techniques have been introduced for the evaluation of wing-body combinations. An excellent review of the state of the art in this field is given by Ashley and Rodden (Ref. 5) and therefore is not repeated here. It may be noted however that, as pointed out in Ref. 5, these newly developed techniques "are really just another evolutionary step toward the remote goal of flow-field analysis for wholly arbitrary configurations". On the other hand, arbitrary

---

* See Ref. 6

configurations have to be considered for aircraft design. Therefore methods for completely arbitrary configurations are becoming more and more important. A general method, suitable for use in automated design is presented here. A brief summary of this method is presented in the rest of this Subsection. The mathematical formulation of the problem is outlined in Subsection 1.2, while an outline of the report is given in Subsection 1.3.

A general theory of the unsteady compressible potential flow around lifting bodies having arbitrary configurations and motions is presented in Ref. 6. In particular, for steady subsonic flow, the theory yields an integral equation relating the potential on the surfaces of the body to the "normal-wash". However, the integral equation becomes singular as wing thickness goes to zero. Hence, in order to demonstrate the feasibility of the method, the problem of a rectangular thin wing is solved numerically herein. The method used consists of dividing the surface of the wing into N small elements, and approximating each element with its tangent plane at the centroid of the element (discrete element method). Then, assuming φ to be constant within each element and satisfying the integral equation at the centroid of the element, yields a system of N linear equations with N unknowns, the values, φ_i , of the potential at the centroids of the elements. The results indicate that the method can be

used even for very small thickness (i.e., thickness ratio τ =.1%. Loss of significant figures becomes important only when τ decreases below about .01%. However, even for τ =.01% the final results are in agreement (to plotting accuracy) with the existing ones.

It may be noted, however, that for thick wings and bodies, the tangent-plane approximation may not be an accurate one. Furthermore, the discrete element method is not necessarily the best method. These questions are analyzed in Ref. 7 where different numerical procedures are considered. These include a "modal method" (as an alternative to the discrete element method) whereby the unknown function φ is expressed as a linear combination of prescribed functions (modes) with unknown coefficients. The results indicate that the discrete element method is preferable for both accuracy and computer time. Variations of the discrete element method are also considered in Ref. 7. These include a purely numerical coefficient (without tangent-plane approximation) as well as a correction (through numerical evaluation of the difference) of the error introduced with the tangent-plane approximation. Results indicate that the last procedure is the most accurate one. However, the improved accuracy does not compensate for the increase in computer time. In other words, if the comparison is made with equal computer time (rather than with equal number of unknowns) the pure tangent-plane approximation is more accurate (for τ =10%) than the corrected tangent-

plane approximation. Hence, the former one is used here although the second one is also mentioned for the sake of completeness.

1.2 Formulation of the Problem

In the following, the isentropic inviscid flow of a perfect gas, initially irrotational, is considered. Under this hypothesis, the flow can be described by the velocity potential Φ . Consider a frame of reference such that the undisturbed flow has velocity U_∞ in the direction of the positive x-axis. Then, it is convenient to introduce the perturbation potential φ , such that

$$\Phi = U_\infty (x + \varphi) \tag{1.1}$$

Note that $\varphi \equiv 0$ in the undisturbed flow. The equation for the linearized potential subsonic aerodynamic flow is,

$$\nabla^2 \varphi = M^2 \frac{\partial^2 \varphi}{\partial x^2} \tag{1.2}$$

where ∇^2 is the Laplacian in x,y,z variables, and

$$M = U_\infty / a_\infty \tag{1.3}$$

is the Mach number.

A very general approach is considered here by assuming that the body immersed in this flow has arbitrary shape. Thus, the surface of the body is represented in the general form,

$$S_B (x, y, z) = 0 \tag{1.4}$$

where the subscript B stands for Body. The boundary condition on the body is given by,

$$\nabla \Phi \cdot \nabla S_B = 0 \tag{1.5}$$

By using Eq. (1.1), Eq. (1.5) yields,

$$\nabla \varphi \cdot \nabla S_B = - \partial S_B / \partial x \tag{1.6}$$

or

$$\frac{\partial \varphi}{\partial n} = \varphi_n \tag{1.7}$$

with

$$\varphi_n = - \frac{1}{|\nabla S_B|} \frac{\partial S_B}{\partial x} \tag{1.8}$$

Furthermore, as mentioned above, the boundary condition at infinity is given by

$$\varphi \equiv 0 \tag{1.9}$$

Finally, the pressure can be evaluated from the Bernoulli Theorem,

$$\frac{p}{p_\infty} = \left[1 - \frac{\gamma - 1}{2 a_\infty^2} \left(\nabla \Phi \cdot \nabla \Phi - U_\infty^2 \right) \right]^{\gamma / \gamma - 1} \tag{1.10}$$

or the linearized Bernoulli Theorem,

$$p - p_\infty = - \rho_\infty U_\infty^2 \frac{\partial \varphi}{\partial x} \tag{1.11}$$

which yields, for the pressure coefficient,

$$C_p = \frac{p - p_\infty}{\frac{1}{2} \rho_\infty U_\infty^2} = - 2 \frac{\partial \varphi}{\partial x} \tag{1.12}$$

1.3 Outline of Report

The method of solution presented here is based upon the well known Green function technique. The Green function for the subsonic flow is used in Section 2 to derive an integral representation of the potential φ at any point in the field (control point) in terms of the values of φ and $\partial\varphi/\partial n$ on a surface surrounding the body and the wake. It is shown in Section 2 that the integral representation can be simplified under the assumption of small perturbation.

In Section 3, the problem of a finite thickness wing in subsonic flow is analyzed within the limits of small-perturbation assumption, that is, linearized potential equation, boundary condition, and Bernoulli's theorem are used. Note that the surface of the body is not modified in view of the fact that the method is intended for complex configuration analysis. It is shown (Appendix A), that if the control point is on the surface of the body, the problem reduces to an integral equation. The question of existence and uniqueness is also discussed in Section 3. In Section 4, the numerical procedure for solving the integral equation is presented. In particular, it is shown that, for a zero-thickness flat wing, the operator becomes singular.

Hence, in order to verify the limit of applicability for low values of the thickness ratio, the subsonic flow around thin wings is solved numerically. The results are presented in Section 5, where the conclusions are discussed also.

SECTION 2

INTEGRAL REPRESENTATION FOR THE VELOCITY POTENTIAL IN SUBSONIC FLOW

2.1 Prandtl-Glauert Transformation

In order to obtain a formally simpler expression for Eq. (1.2), the following Prandtl-Glauert Transformation is made,

$$X = x/\beta \qquad Y = y \qquad Z = z \tag{2.1}$$

where

$$\beta = (1 - M^2)^{1/2} \tag{2.2}$$

Using these new coordinates, Eq. (1.2) can be rewritten as,

$$\bar{\nabla}^2 \varphi = 0 \tag{2.3}$$

where $\bar{\nabla}$ is defined as,

$$\bar{\nabla} = \frac{\partial}{\partial X}\vec{I} + \frac{\partial}{\partial Y}\vec{J} + \frac{\partial}{\partial Z}\vec{K} \tag{2.4}$$

Thus Eq. (1.2) is reduced to a Laplace equation. Eq. (2.3) is solved by the well known Green function technique, which will briefly be shown in the following subsection.

2.2 Green's Theorem for the Laplace Equation

The Green's function for Eq. (2.3) is defined as a function satisfying the following equation,

$$\bar{\nabla}^2 G = \delta(X - X_1, Y - Y_1, Z - Z_1) \tag{2.5}$$

where δ is the Dirac delta function.

Multiplying Eq. (2.3) by G and subtracting from it Eq. (2.5) multiplied by φ , one obtains,

$$G\bar{\nabla}^2\varphi - \varphi\bar{\nabla}^2 G = -\varphi\delta \tag{2.6}$$

Making use of the identity,

$$\bar{\nabla}\cdot(a\bar{\nabla}b) = \bar{\nabla}a\cdot\bar{\nabla}b + a\bar{\nabla}^2 b \tag{2.7}$$

one obtains,

$$\bar{\nabla}\cdot(G\bar{\nabla}\varphi - \varphi\bar{\nabla}G) = -\varphi\delta \tag{2.8}$$

Defining a field function E such that,

$$\begin{aligned} E &= 1 \quad \text{in V (outside of body)} \\ &= 0 \quad \text{otherwise} \end{aligned} \tag{2.9}$$

and multiplying Eq. (2.8) by E, then integrating it over V, one obtains,

$$\iiint_V E\,\bar{\nabla}_1\cdot(G\bar{\nabla}_1\varphi - \varphi\bar{\nabla}_1 G)\,dV_1 = -\iiint_V E\,\varphi\,\delta\,dV_1 \tag{2.10}$$

Using the following identities,

$$\iiint_V \bar{\nabla}\cdot\vec{V}\,dV_1 = \oiint \vec{V}\cdot\vec{N}_1\,d\Sigma_1 \tag{2.11}$$

$$\iiint_V a\,\delta(x-x_1, Y-Y_1, Z-Z_1)\,dV_1 = a(x, Y, Z) \tag{2.12}$$

with

$$\vec{N}_1 = \frac{\bar{\nabla}_1 S}{|\bar{\nabla}_1 S|} \tag{2.13}$$

and noting that the solution to Eq. (2.5) is,[8]

$$G = -\frac{1}{4\pi R} \tag{2.14}$$

with

$$R = [(X-X_1)^2 + (Y-Y_1)^2 + (Z-Z_1)^2]^{1/2} \tag{2.15}$$

Eq. (2.10) then becomes,

$$4\pi E \varphi = \iint_{\Sigma} [\varphi \frac{\partial}{\partial N_1}(\frac{1}{R}) - \frac{1}{R} \varphi_N] d\Sigma \tag{2.16}$$

where

$$\varphi_N = \frac{\partial \varphi}{\partial N_1} = \frac{\bar{\nabla}_1 S}{|\bar{\nabla}_1 S|} \cdot \bar{\nabla}_1 \varphi \tag{2.17}$$

Eq. (2.16) is the desired integral representation for the velocity potential φ .

2.3 Small Perturbation Hypothesis

In this subsection, considerable simplification of Eq. (2.16) is obtained by making use of the small perturbation hypothesis. It should be noted that the small perturbation hypothesis has been evoked by assuming that the governing equation of motion is represented by the linearized equation of the velocity potential as shown in Eq. (1.2). For neglecting of nonlinear terms implies that the derivatives of φ are much smaller than one, i.e., in compact form,

$$\frac{\varphi}{L} = O(\bar{\epsilon}) << 1 \tag{2.18}$$

where L is a characteristic length of the problem.

This hypothesis is now used to simplify Eq. (2.16) into,

$$4\pi E \varphi = \iint_{\Sigma} \left[\varphi \frac{\partial}{\partial N_1} \left(\frac{1}{R} \right) - \varphi_n \frac{1}{R} \right] d\Sigma \tag{2.19}$$

where φ_n is defined in Eq. (1.7).

In order to do this, consider the boundary condition given by Eq. (1.6). Under the assumption of small perturbation,

$$\frac{\partial \varphi}{\partial n} = O(\bar{\epsilon}) << 1 \tag{2.20}$$

or, according to Eq. (1.8),

$$\frac{1}{|\nabla S|} \frac{\partial S}{\partial x} = O(\bar{\epsilon}) << 1 \tag{2.21}$$

This means that the x-component of the normal is small compared to the other two, hence

$$|\bar{\nabla} S| \cong |\nabla S| \tag{2.22}$$

and

$$\begin{aligned} \varphi_N &= \frac{\bar{\nabla}\varphi \cdot \bar{\nabla} S}{|\bar{\nabla} S|} = \frac{\nabla\varphi \cdot \nabla S}{|\bar{\nabla} S|} - M^2 \frac{\partial \varphi}{\partial x} \cdot \frac{\partial S}{\partial x} \frac{1}{|\bar{\nabla} S|} \\ &\cong \frac{\nabla\varphi \cdot \nabla S}{|\nabla S|} = \varphi_n \end{aligned} \tag{2.23}$$

Hence, Eq. (2.16) can be approximated by Eq. (2.19).

SECTION 3

NUMERICAL FORMULATION

3.1 Introduction

In the preceding sections, a brief discussion of the theory of steady subsonic flow is given. In Section 1, the problem is formulated. In Section 2, the Green Function technique is applied to obtain the integral representation for the velocity potential φ , i.e., φ at any field point is related to φ and $\frac{\partial \varphi}{\partial n}$ on the surface of the body and the wake. A simplified expression is then obtained under the hypothesis of small perturbations.

It is obvious that the general formulation presented here has no closed-form solution except for a few very special cases. Hence, in general, the use of high speed computers will be required. Thus, the numerical solution of the problem as formulated in Subsection 2.3 (small perturbation flow around an arbitrary wing) is discussed here. It should be mentioned that the numerical problems arise especially on the treatment of a thin wing (see Subsection 4.6). Thus, in the discussion, it will be assumed that the body under consideration is a thin wing, although the formulation is valid for any body with sharp trailing edges (see Subsection 3.3).

3.2 Integral Equation Formulation; Existence and Uniqueness of the Solution

The integral representation of the potential for steady compressible flow in Prandtl-Glauert variables is given by (see Eq. 2.19),

$$4\pi E\varphi = -\iint_{\Sigma} \varphi_n \frac{1}{R} d\Sigma + \iint_{\Sigma} \varphi \frac{\partial}{\partial N_1}\left(\frac{1}{R}\right) d\Sigma \qquad (3.1)$$

In order to analyze the question of uniqueness of the solution, the surface Σ is replaced by a smooth surface Σ' surrounding (at very small, but finite, distance; the boundary layer thickness, for instance) the body and the wake (Fig. 2a). The wake is truncated at a very large, but finite, distance from the wing. If the control point is on the surface Σ', the function E assumes the value 1/2 and Eq. (3.1) reduces to,*

$$2\pi\varphi = -\iint_{\Sigma'} \varphi_n \frac{1}{R} d\Sigma' + \iint_{\Sigma'} \varphi \frac{\partial}{\partial N_1}\left(\frac{1}{R}\right) d\Sigma' \qquad (3.2)$$

If the geometry of the wake is known and if φ_n is replaced by the value (see Eq. 1.8),

$$\varphi_n = \frac{\partial \varphi}{\partial n} = -\partial S/\partial x_1 \Big/ |\nabla_1 S| \qquad (3.3)$$

which assumes on the body and the wake, then Eq. (3.2) is an

---

*See Appendix A

integral equation relating the downwash integral to the unknown value of φ on the surface. Note that Eq. (3.2) gives the solution of the exterior Neumann problem and, in this case, the solution of the equation exists and is unique*, for any smooth (Lyapunov) surface (Ref. [9], pp. 620-621).

Next, the surface Σ' (surrounding the body and the wake) is replaced by the surface Σ, composed of two branches, the surface Σ_B of the body and the surface Σ_W of the wake (Fig. 2b). Thus, Eq. (3.2), combined with Eq. (3.3), reduces to**

$$2\pi\varphi = -\oint\!\!\!\!\!\!\diagup_{\Sigma_B} \varphi_n \frac{1}{R}\, d\Sigma + \oint\!\!\!\!\!\!\diagup_{\Sigma_B} \varphi \frac{\partial}{\partial N_1}\left(\frac{1}{R}\right) d\Sigma + \iint_{U^W} (\varphi_u - \varphi_\ell) \frac{\partial}{\partial N_1}\left(\frac{1}{R}\right) d\Sigma \tag{3.4}$$

In Eq. (3.4), U^W is the upper side of the surface of the wake and hence, the normal $\vec{N}_1$ is understood to be the upper normal.

---

*Note that, for the interior Neumann problem, the solution of the equation is not unique, for any arbitrary constant can be added to the solution. Physically speaking, one might say that, for the exterior problem, this arbitrariness is eliminated by the condition $\varphi = 0$ at infinity.

**The source integral on the wake is equal to zero.

Note that only the value of φ_n on the surface of the body (not on the wake) is necessary to solve the integral Equation (3.4).

From physical considerations, the solution of Eq. (3.4) is "very close" to the one of Eq. 3.2. Thus, it will be assumed that, if the geometry of the wake is known, the solution of Eq. (3.4) exists and is unique. It should be emphasized however, that this conclusion is based upon physical reasoning. However, this reasoning is questionable, as shown by the remarks given in Subsection 4.6. Hence, a rigorous mathematical proof of the existence and uniqueness of the solution of Eq. (3.4) would be highly desirable.

However, there are still two important questions to be considered: first, the geometry of the wake and second, the special behaviour of Eq. (3.4) when the thickness of the wing goes to zero. These two questions are discussed in Subsection 3.3 and 4.6, respectively.

3.3 The Wake

As mentioned in the preceding subsection, the surface of the wake in Eq. (3.4) is not known. Thus, Eq. (3.4), which is satisfied on the body, must be completed by the equation on the wake, which says that the velocity on the wake is tangent to the surface of the wake. Thus, one obtains two coupled integral equations, one on the body and one on the wake, with φ unknown on the body and φ_n unknown on

the wake, whereas φ_n is known on the body and $\Delta\varphi = \varphi_u - \varphi_l$ is constant along the x-direction on the wake, since no pressure discontinuity can exist across the wake:

$$\Delta C_p = -2 \frac{\partial}{\partial x} \Delta\varphi = 0 \tag{3.5}$$

According to the Kutta condition, this constant value is equal to the value of $\Delta\varphi$ at the trailing edge. Given the velocity on the wake, the geometry of the wake is obtained by the condition that the velocity is tangent to the wake. This approach has been successfully used in Ref.10 to study the transient incompressible flow around a wing after a sudden start. However, from a practical point of view, this approach is too lengthy and a simplified treatment of the contribution of the wake is presented in the following.

Note first that

$$\iint \frac{\partial}{\partial N_1}\left(\frac{1}{R}\right) d\Sigma = -\iint \frac{\vec{N}\cdot\vec{R}}{R^2 \cdot R} d\Sigma = -\iint \frac{d\Sigma_n}{R^2} = -\iint d\Omega \tag{3.6}$$

where

$$d\Sigma_n = d\Sigma \cos\angle(\vec{N}, \vec{R}) \tag{3.7}$$

is the projected area (along the direction $\vec{R}$) and

$$d\Omega = \frac{d\Sigma_n}{R^2} \tag{3.8}$$

is the solid angle (see Fig. 3).

Next, consider the wake integral as a sum of M strips in the x direction (see Fig. 4). Applying the mean value

theorem, one obtains (note that $\Delta\varphi$ is only the function of Y_1),

$$I_W = \iint_{U^W} \Delta\varphi(Y_1) \frac{\partial}{\partial N_1}\left(\frac{1}{R}\right) d\Sigma = -\iint_{U^W} \Delta\varphi(Y_1)\, d\Omega$$

$$= -\sum_{m=1}^{M} \Delta\varphi(Y_{1m}) \iint_{U_m^W} d\Omega = -\sum_{m=1}^{M} \Delta\varphi(Y_{1m})\Omega_m \qquad (3.9)$$

where $\Delta\varphi(Y_{1m})$ are the mean values of $\Delta\varphi$ for each strip U_m^W, and Ω_m are the solid angles of the strip U_m^W. Eq. (3.9) shows that any changes of the wake such that solid angles Ω_m are not altered, do not have any influence on the value of the wake integral I_W.

This suggests that a "reasonable" geometry for the wake can be assumed, provided that the values of the associated solid angles are not excessively different from the true ones. Hence, it is possible (and convenient) to approximate the wake by straight vortex-lines, parallel to the direction of the flow, emanating from the trailing edge of the wing*. For, geometrical considerations show that the solid angles, Ω_m, are changed only slightly. With this assumption, the wake integral simplifies considerably and its contribution reduces to a line integral. For if the trailing edge is given by

$$X = X_{T.E.}(Y)$$
$$Z = Z_{T.E.}(Y) \qquad (3.10)$$

then the equation of the surface of the wake is given by

$$S \equiv Z_1 - Z_{T.E.}(Y_1) = 0 \qquad (3.11)$$

*This is consistent with the small-perturbation assumption. The limiting behaviour as the thickness of the wing approaches zero is discussed in Ref. 6, Appendix G (See also Subsection 4.7 of this report).

and

$$I_w = -\int_{-b/2}^{b/2} d\gamma_1 \int_{x_{T.E.}}^{\infty} \Delta\varphi \,(\nabla_1 S \cdot \vec{R})\, \frac{1}{R^3}\, dx_1 d\gamma_1$$
$$= \int_{-b/2}^{b/2} \Delta\varphi\, J_w\, d\gamma_1 \qquad (3.12)$$

where b is the span of the wing and

$$J_w = \left[(z_1 - z) - \frac{dz_{T.E.}}{d\gamma_1}(\gamma_1 - \gamma)\right] \int_{x_{T.E.}}^{\infty} \frac{-1}{R^3}\, dx_1$$
$$= \left[(z_1 - z) - \frac{dz_{T.E.}}{d\gamma_1}(\gamma_1 - \gamma)\right] \frac{-1}{(\gamma_1-\gamma)^2 + (z_1 - z)^2}\left[1 - \left(\frac{x_{T.E.} - x}{R}\right)\right] \qquad (3.13)$$

with $z_1 = z_{T.E.}(\gamma_1)$. In particular, if the trailing edge is in the plane $z_1 = 0$ (i.e., $z_{T.E.}(\gamma_1) \equiv 0$), Eq. (3.13) reduces to

$$J_w = \frac{z}{(\gamma_1-\gamma)^2 + z^2}\left\{1 - \frac{x_{T.E.} - x}{\left[(x_{T.E.}-x)^2 + (\gamma_1-\gamma)^2 + (z_1 - z)^2\right]^{1/2}}\right\} \qquad (3.14)$$

In conclusion, under the reasonable assumption of cylindrical wake (straight vortex-lines) the effect of the wake simplifies considerably and Eq. (3.4) reduces to,

$$2\pi\varphi = \iint_{\Sigma} \varphi_n \frac{1}{R}\, d\Sigma + \iint_{\Sigma} \varphi \frac{\partial}{\partial N_1}\left(\frac{1}{R}\right) d\Sigma$$
$$+ \int_{-b/2}^{b/2} \Delta\varphi_{T.E.}\, J_w\, d\gamma_1 \qquad (3.15)$$

with J_w given by Eq. (3.13).

Finally, an important remark about bodies without sharp trailing edges, must be made. In the discussion presented in

this subsection, it was assumed that the wing had a sharp trailing edge. Note that the results can be easily generalized to the case of general bodies with sharp trailing edges. However, for bodies without sharp trailing edges, the inviscid flow theory is incapable, in general, of predicting the location of the stagnation point from which the wake emanates. This can be easily seen in the case of rotating cylinder of finite length. From the experiments the location of the stagnation point depends upon the angular velocity, ω . On the other hand, the equation of the geometry of the cylinder does not depend upon ω and thus ω does not even appear in the equation of the inviscid flow.

In the following, it is assumed that the body under consideration has a sharp trailing edge. However, a viscous theory which predicts the location of the stagnation point from which the wake emanates, is necessary in order to extend this method to bodies without sharp trailing edges. Similar consideration holds for the case of detached flow (when this can be approximated by a wake emanating from a point different from the sharp trailing edge).

SECTION 4

NUMERICAL PROCEDURE

4.1 Discrete Element Formulation

The governing equation for the velocity potential, after Prandtl-Glauert transformation, for steady subsonic flow, is shown in Eq. (2.19) and is rewritten here,

$$4\pi E\varphi = -\oint\!\!\!\!\!\!\diagup_{\Sigma} \varphi_n \frac{1}{R} d\Sigma + \oint\!\!\!\!\!\!\diagup_{\Sigma} \frac{\partial}{\partial N_1}\left(\frac{1}{R}\right)\varphi\, d\Sigma \tag{4.1}$$

where φ on the left hand side, represents the velocity potential at a field point P and φ on the right hand side represents the potential at a point P_1 on the boundaries (body surfaces and wake). E is defined as,

$$\begin{aligned} E &= 0 \quad && \text{if P is inside the body} \\ &= 1/2 && \text{if P is on the surface} \\ &= 1 && \text{if P is outside of the body} \end{aligned} \tag{4.2}$$

From Eq. (4.1), it can be seen that if φ on the boundaries is known, the velocity potential at any field point can be obtained immediately. So the first step is to find φ on the boundaries. With E = 1/2, Eq. (4.1) becomes,

$$\begin{aligned} 2\pi\varphi = &-\oint\!\!\!\!\!\!\diagup_{\Sigma_B} \varphi_n \frac{1}{R} d\Sigma + \oint\!\!\!\!\!\!\diagup_{\Sigma_B} \varphi \frac{\partial}{\partial N_1}\left(\frac{1}{R}\right) d\Sigma \\ &+ \iint_{U^W} \Delta\varphi \frac{\partial}{\partial N_1}\left(\frac{1}{R}\right) d\Sigma \end{aligned} \tag{4.3}$$

where Σ_B is the surface of the lifting body, U^W is the upper surface of the wake and,

$$\Delta\varphi = (\varphi_{upper} - \varphi_{lower}) \tag{4.4}$$

on the wake. Eq. (4.3) cannot be solved analytically except for some special cases. Hence, numerical scheme has to be employed. The procedure used in this study is as follows. As mentioned in Section 3, the wake is approximated by a plane parallel to the direction of flow, and $\Delta\varphi$ on the wake is equal to $\Delta\varphi$ at the trailing edge and integration in the x-direction from $x = x_{T.E.}$ to $x \to \infty$ is carried out as outlined in Section 3.3. Secondly, the surface of the body is divided into discrete surface elements (see Fig. 4). In each element, φ is approximated by its value at the centroid of the element, then the integration is carried out within each element. The resulting equation can be written as

$$\varphi_k = b_k + \sum_{i=1}^{N} c_{ki}\,\varphi_i + \sum_{i=1}^{N} w_{ki}\,\varphi_i \tag{4.5}$$

with

$$b_k = -\iint_{\Sigma} \varphi_n \frac{1}{2\pi R_k}\, d\Sigma \tag{4.6}$$

$$c_{ki} = \iint_{\Sigma_i} \frac{\partial}{\partial N_1}\left(\frac{1}{2\pi R_k}\right) d\Sigma_i \tag{4.7}$$

where

$$R_k = \left[(X^{(k)} - X_1)^2 + (Y^{(k)} - Y_1)^2 + (Z^{(k)} - Z_1)^2\right]^{1/2} \tag{4.8}$$

is the distance between the dummy point of integration P_1 to the center point $P^{(k)}$ of the element k, and

$$w_{ki} = W_i|_{P=P^{(k)}} = \left\{\int_{\Delta y_i} J_W\, dY_1\right\}_{P=P^{(k)}} \tag{4.9}$$

for the boxes in contact with the trailing edge and

$$w_{ki} = 0 \tag{4.10}$$

otherwise. Eq. (4.5) can be rewritten as

$$\sum_{i=1}^{N} a_{ki}\,\varphi_i = b_k \tag{4.11}$$

with

$$a_{ki} = \delta_{ki} - c_{ki} - w_{ki} \tag{4.12}$$

where δ_{ki} is the Kronecker delta. Solving Eq. (4.11), one obtains the solution of the problem. So the question which remains now is how to evaluate b_k, c_{ki}, and w_{ki}.

For a wing symmetric about the plane $Y = 0$, Eq. (4.10) can be rewritten as

$$\sum_{i=1}^{\hat{N}} \hat{a}_{ki}\,\varphi_i = \sum_{i=1}^{\hat{N}} (\delta_{ki} - \hat{c}_{ki} - \hat{w}_{ki})\,\varphi_i = b_k \tag{4.13}$$

where $\hat{N} = N/2$ is the total number of elements on the right hand part of the wing and c_{ki} is the influence of two elements (in symmetric position with respect to the plane $Y = 0$) on an element on the right hand part of the wing,

$$\hat{c}_{kl} = \frac{1}{2\pi} \oint_{\Sigma_i^{(R)}} \left[\frac{\partial}{\partial N_1}\left(\frac{1}{R_k}\right)\right]_{(R)} d\Sigma_i^{(R)} + \frac{1}{2\pi} \oint_{\Sigma_i^{(L)}} \left[\frac{\partial}{\partial N_1}\left(\frac{1}{R_k}\right)\right]_{(L)} d\Sigma_i^{(L)} \tag{4.14}$$

with

$$\left[\frac{\partial}{\partial N_1}\left(\frac{1}{R_k}\right)\right]_R = \frac{-1}{|\nabla_1 S|}\left[\frac{\partial S}{\partial X_1}(X_1 - X) + \frac{\partial S}{\partial Y_1}(Y_1 - Y) + \frac{\partial S}{\partial Z_1}(Z_1 - Z)\right] \tag{4.15a}$$

$$\times \left(\frac{1}{R_k^{(R)}}\right)^3$$

$$\left[\frac{\partial}{\partial N_1}\left(\frac{1}{R_k}\right)\right]_{(L)} = \frac{-1}{|\nabla_1 S|}\left[\frac{\partial S}{\partial X_1}(X_1 - X) + \frac{\partial S}{\partial Y_1}(Y_1 + Y) + \frac{\partial S}{\partial Z_1}(Z_1 - Z)\right] \times \left(\frac{1}{R_k^{(L)}}\right)^3 \tag{4.15b}$$

where

$$R_k^{(R)} = \left[(X_1 - X)^2 + (Y_1 - Y)^2 + (Z_1 - Z)^2\right]^{1/2}$$
$$R_k^{(L)} = \left[(X_1 - X)^2 + (Y_1 + Y)^2 + (Z_1 - Z)^2\right]^{1/2} \tag{4.16}$$

Similar expression holds for w_{ki}.

Evaluation of c_{ki}, w_{ki} and b_k is shown as follows.

4.2 The Geometry of the Wing

The planform of the wing is defined as

$$\bar{x}_{T.E.} = \bar{x}_{T.E.}(\bar{y}) \tag{4.17}$$

$$\bar{x}_{L.E.} = \bar{x}_{L.E.}(\bar{y}) \qquad \text{for } 0 < \bar{y} < b/2 \tag{4.18}$$

where b is the span of the wing. The chord of the wing at any point is then defined as

$$c(\bar{y}) = \bar{x}_{T.E.}(\bar{y}) - \bar{x}_{L.E.}(\bar{y}) \tag{4.19}$$

This planform can be transformed into a rectangular one by the following transformation

$$\xi = \frac{\bar{x} - \bar{x}_{L.E.}}{\bar{x}_{T.E.} - \bar{x}_{L.E.}} \qquad 0 \le \xi \le 1 \tag{4.20}$$

$$\eta = 2\bar{y}/b \qquad -1 \le \eta \le 1 \tag{4.21}$$

The thickness, h, of the wing is defined as

$$h = \tau\, c_{max} \frac{3\sqrt{3}}{2} \sqrt{\zeta}\,(1-\zeta)\sqrt{1-\eta^2} \tag{4.22}$$

where c_{max} is the maximum chord length and τ is the thickness ratio of the wing, i.e.,

$$\tau = \frac{h_{max.}}{c_{max.}} \tag{4.23}$$

Summing up, the geometry of the wing is represented by

$$\begin{aligned} \bar{x} &= (x_{T.E.} - x_{L.E.})\,\zeta + x_{L.E.} \\ \bar{y} &= b\eta/2 \\ \bar{z} &= \pm \tau\, c_{max} \frac{3\sqrt{3}}{4} \sqrt{\zeta}\,(1-\zeta)\sqrt{1-\eta^2} \end{aligned} \tag{4.24}$$

$$\text{for} \quad 0 \le \zeta \le 1 \qquad -1 \le \eta \le 1$$

If the angle of attack α is different from zero, then

$$\begin{aligned} x &= \bar{x}\cos\alpha + \bar{z}\sin\alpha \\ y &= \bar{y} \\ z &= -\bar{x}\sin\alpha + \bar{z}\cos\alpha \end{aligned} \tag{4.25}$$

For small τ and α , Eq. (4.25) can be approximated by

$$\begin{aligned} x &= \bar{x} \\ y &= \bar{y} \\ z &= \bar{z} - x\alpha \end{aligned} \tag{4.26}$$

As mentioned before, in the process of solving Eq. (4.4), the wing is divided into elements and the mean value of φ inside each element is approximated by that at the centroid of the element. Because φ and the slopes of the wing vary more

rapidly near the leading edge and the tips, smaller elements are required at these regions. Using the following transformation,

$$\xi = \bar{X}^2$$
$$\eta = 1 - (1-\bar{Y})^2 \tag{4.27}$$

then, dividing the transformed planform into even mesh (i.e., the mesh size is

$$\Delta\bar{X} = 1/NX$$
$$\Delta\bar{Y} = 1/NY \tag{4.28}$$

where NX and NY are the numbers of elements in the x and y directions, respectively), the boundary of the element on the n_x row and n_y column is

$$(n_x-1)\,\Delta\bar{X} \le \bar{X} \le n_x\,\Delta\bar{X}$$
$$(n_y-1)\,\Delta\bar{Y} \le \bar{Y} \le n_y\,\Delta\bar{Y} \tag{4.29}$$

The centroid of this element is defined as

$$\bar{X}_c = (n_x - .5)\,\Delta\bar{X}$$
$$\bar{Y}_c = (n_y - .5)\,\Delta\bar{Y} \tag{4.30}$$

Note that Eqs. (4.28) and (4.29) yield smaller elements near the leading edge and tips.

4.3 Calculation of c_{ki}

The evaluation of c_{ki} consists of two parts. The first part is to approximate the wing by replacing each element by a plane tangent to the wing at the centroid of the element defined in Eq. (4.30). The boundary of the tangent plane is

defined by Eq. (4.29). The equation of the tangent plane can be written as

$$z - z_c = \left(\frac{\partial z}{\partial x}\right)_c (x - x_c) + \left(\frac{\partial z}{\partial y}\right)_c (y - y_c) \qquad (4.31)$$

where the subscript "c" indicates the value at the centroid mentioned before.

The integration of Eq. (4.14) on these tangent planes can be carried out analytically as shown in Appendix B. This tangent plane approximation yields good results for thin wing (thickness ratio varying from .1% to 1.%). The computer time required for this tangent plane approximation ranges from 13 sec. for NX = NY = 4 to 128 sec. for NX = NY = 7, on the IBM 360/50 of the Boston University computing center.

For a thick wing, the tangent plane approximation may not yield good results. Then the solution can be improved in the following manner. The most severe error comes from two sources. First, the curvature of the surface changes very rapidly near the leading edge and the tips. So, the tangent plane is not a good representation of the true surface. Secondly, as can be seen from Eq. (4.16), $R_k^{(R)} \approx 0$ when k = i (i.e., field point coincides with source point), so $1/R_k$ in Eq. (4.14) varies rapidly, hence again making the tangent plane a poor approximation. Thus, it is necessary to integrate numerically the difference between the actual surface of the element and the tangent plane; and add this correction value to that of the tangent plane approximation.

The numerical integration scheme used here is the Gaussian quadrature. For integration over the leading edge and the tips (but $i \neq j$), a four point Gaussian quadrature is used. For $i = j$, a polar Guassian quadrature (see Appendix C) is used. The results obtained in Ref. 7 indicate that no correction is needed for the elements which are not on the leading edge nor on tips and are such that $i \neq j$.

4.4 Calculation of w_{ki}

As mentioned before, the surface of the wake is approximated by a surface parallel to the direction of the flow, emanating from the trailing edge of the wing. Based on this assumption, it is shown that Eq. (3.12),

$$\iint \Delta\varphi \frac{\partial}{\partial N_1}\left(\frac{1}{R}\right) d\Sigma = -\int_{-b/2}^{b/2} \Delta\varphi_{T.E.} J_W \, dY_1 \tag{4.32}$$

with

$$J_W = \left[(Z_{T.E.} - Z) - \frac{dZ_{T.E.}}{dY}(Y_1 - Y)\right] \int_{X_{T.E.}}^{\infty} \frac{1}{R^3} dX_1$$

$$= \left[(Z_{T.E.} - Z) - \frac{dZ_{T.E.}}{dY}(Y_1 - Y)\right] \frac{-1}{(Y_1-Y)^2+(Z_1-Z)^2}\left[1 - \left(\frac{X_1 - X}{R}\right)_{X_1 = X_{T.E.}}\right] \tag{4.33}$$

and $\Delta\varphi_{T.E.} = (\varphi_{T.E.})_u - (\varphi_{T.E.})_\ell$. Then, integrate Eq. (4.32) and lump $\Delta\varphi_{T.E.}$ to the last row of elements in contact with the trailing edge. It should be noted that if $dZ/dY \equiv 0$, or if this term is negligible compared to the other term in the same bracket, Eq. (4.32) can be integrated exactly.

4.5 Calculation of b_k

The process of evaluating b_k, i.e., Eq. (4.6), is similar to that for evaluating c_{ki}. For thin and moderately thin wing, b_k is evaluated analytically on the tangent plane approximation. Integration for b_k on these planes is shown in Appendix B. For a thick wing, the solution is improved, as for c_{ki}, by numerically integrating the difference between the real surface and the tangent plane and adding this difference to the value obtained by the tangent plane approximation.

It is worth noting that, for a wing with a plane midsurface (symmetric about this plane), φ_n consists of the symmetric part (value on upper surface is same as that on lower surface) and the antisymmetric part. The symmetric part $\varphi_n^{(s)}$ is,

$$\varphi_n^{(s)} = \pm\left(\frac{\partial z}{\partial x}\right) = \left|\frac{\partial z}{\partial x}\right| \tag{4.34}$$

and the antisymmetric part $\varphi_n^{(a)}$ is,

$$\varphi_n^{(a)} = \pm\alpha \tag{4.35}$$

where the upper sign stands for upper surface and the lower sign for lower surface. Since b_k is linearly proportional to φ_n, b_k can be separated into symmetric part and antisymmetric part. Eq. (4.11) can be rewritten in two equations,

$$a_{ki}\,\varphi_i^{(s)} = b_k^{(s)} \tag{4.36}$$

$$a_{ki}\,\varphi_i^{(a)} = b_k^{(a)} \tag{4.37}$$

where $\varphi_i^{(s)}$ stands for the symmetric solution and $\varphi_i^{(a)}$ for anti-symmetric solution. Separation of φ_i into these two parts avoids elimination of significant figure due to the presence of the other, hence greatly improves the accuracy of the solution.

4.6 Calculation of the Pressure Coefficient C_p

As shown in Eq. (1.12), the pressure coefficient can be written as

$$C_p = -2\,\partial\varphi/\partial x \tag{4.38}$$

As a first approximation, C_p is evaluated by finite difference method, i.e.,

$$(C_p)_i = -2\left(\frac{\varphi_{i+1}-\varphi_i}{\Delta x_i}\right) = -2\,\frac{\varphi_{i+1}-\varphi_i}{\Delta\bar{x}}\,\frac{1}{2\bar{X}_i c} \tag{4.39}$$

where $(C_p)_i$ is the C_p at the rear end of the element on the ith row, φ_i is the value of φ at the centroid of the element on the ith row and Δx_i is the distance, in the x-direction, between the centroids of the ith and i + 1st rows of elements.

A better approximation for C_p is to combine Eqs. (4.1) and (4.38) and calculate C_p by integration. For the present purpose, however, Eq. (4.39) is a good approximation.

4.7 Limiting Behavior for Zero Thickness

As mentioned above, the formulation described thus far becomes singular in the case of zero thickness. This is

shown clearly by the fact that, for lifting surface (in the plane $z_1 = 0$), Eq. (4.1) reduces to

$$2\pi \varphi_u = -\iint_{\Sigma^{(w)}} (\varphi_u - \varphi_\ell) \frac{\partial}{\partial Z} \left(\frac{1}{R}\right)_{Z_1=0} dX_1 dY_1 \tag{4.40}$$

and

$$2\pi \varphi_\ell = \iint_{\Sigma^{(u)}} (\varphi_u - \varphi_\ell) \frac{\partial}{\partial Z} \left(\frac{1}{R}\right)_{Z_1=0} dX_1 dY_1 \tag{4.41}$$

where $\Sigma^{(w)}$ is the portion of the plane $Z_1 = 0$ (upper side) which contains the wing and the wake. By adding and subtracting Eqs. (4.40) and (4.41), one obtains

$$\varphi_u + \varphi_\ell = 0 \tag{4.42}$$

and

$$2\pi \Delta\varphi + \iint_{\Sigma^{(w)}} \Delta\varphi \frac{\partial}{\partial Z} \left(\frac{1}{R}\right)_{Z_1=0} dX_1 dY_1 = 0 \tag{4.43}$$

This implies that (since, as well known, there exists a non-trivial solution $\Delta\varphi \neq 0$) the operator shown in Eq. (4.43) is singular.

Hence, one can expect that the numerical procedure also has a singular behavior. In order to show that this is indeed the case, consider a symmetric wing with angle of attack α and thickness ratio τ, and let τ go to zero. In this case, Eq. (4.6) shows that

$$\lim_{\tau \to 0} b_k = 0 \tag{4.44}$$

since $(\varphi_n)_u = -(\varphi_n)_\ell$. In order to simplify the discussion,

the numbering of the elements is assumed to be such that the odd (even) numbers correspond to elements in the upper (lower) surface and that the element in opposite position to the upper element i, has the number i + 1 (see Fig. 4). As before, upper element i and lower element i + 1 will be called "opposite elements".

With this numbering, it is easy to show[6] that, according to Eq. (4.7),

$$\lim_{\tau \to 0} [C_{ki}] = \begin{bmatrix} 0 & -1 & 0 & 0 & 0 & 0 \\ -1 & 0 & 0 & 0 & 0 & 0 \\ 0 & 0 & 0 & -1 & 0 & 0 \\ 0 & 0 & -1 & 0 & 0 & 0 \\ 0 & 0 & 0 & 0 & 0 & 0 \\ 0 & 0 & 0 & 0 & 0 & -1 \\ 0 & 0 & 0 & 0 & -1 & 0 \end{bmatrix} \tag{4.45}$$

In other words, all the coefficients c_{ik} are equal to zero except for the ones relating opposite elements, which assume the value -1. Furthermore, the coefficients w_{ki} are equal to zero. Hence, Eq. (4.11) in the limit, as τ goes to zero, reduces to

$$\begin{bmatrix} 1 & 1 & 0 & 0 & 0 & 0 \\ 1 & 1 & 0 & 0 & 0 & 0 \\ 0 & 0 & 1 & 1 & 0 & 0 \\ 0 & 0 & 1 & 1 & 0 & 0 \\ 0 & 0 & 0 & 0 & 0 & 0 \\ 0 & 0 & 0 & 0 & 0 & 0 \\ 0 & 0 & 0 & 0 & 0 & 0 \end{bmatrix} \begin{Bmatrix} \varphi_i \end{Bmatrix} = 0 \tag{4.46}$$

This equation can have a nontrivial solution since the determinant is equal to zero.

Note that this result implies that zero thickness wings (lifting surface theory) are more difficult to deal with than finite thickness wings.

However, this shows also that, by using the method proposed here, one may encounter numerical complication due to the fact that, for very thin wings, the determinant is close to zero and hence, one may encounter strong elimination of significant figures. This implies that one has to be very careful in the evaluation of the coefficients c_{ki} and b_k.

In order to establish the practical limits of the applicability of the method, Eq. (4.11) has been solved numerically for very small values of ε . The results are presented in Section 5.

SECTION 5

NUMERICAL RESULTS

5.1 Introduction

Some numerical results showing the validity and flexibility of the present method are shown in this section. The convergence of the present method is analyzed in Subsection 5.2.1. The effect of the numerical correction for a thick wing (as discussed in Subsections 4.2 and 4.4) is discussed in Subsection 5.2.2. The effect of thickness is described in Subsection 5.2.3. Finally, comparison with existing results is given in Subsection 5.3.

To give an idea about the functional type of the solution, the value of φ and C_ℓ are shown in three-dimensional forms in Figs. 5 and 6, where

$$C_\ell = -\Delta C_p = C_{p_\ell} - C_{p_u} \tag{5.1}$$

is the lift coefficient. The thickness ratio is $\tau = .001$, angle of attack $\alpha = 5°$, aspect ratio b/c = 3 and the mesh NX = NY = 7 (that is N = 98). It may be noted that the diagram of C_ℓ is flat in the neighborhood of the root (more precisely $\partial C_\ell / \partial y = 0$ at root). Hence, in the following discussion of convergence, the value of C_ℓ at the centroid of the elements in contact with the root (root elements) is used.

5.2 General Characteristics of the Method

As mentioned above, in this subsection the convergence,

the effects of the numerical correction and of the thickness are analyzed.

5.2.1 Convergence

In order to study the convergence of the solutions, the case $\tau = .001$ was solved for NX = NY = 4, 5, 6 and 7, respectively. The values of the lift distribution $C_\ell = -\Delta C_p$ at the root elements are shown in Fig. 7.

The results show that the solution is convergent very fast and that the case 4 x 4 is sufficient for an accurate analysis. The computer time employed on the IBM 360/50, available at the Boston University Computing Center, is given in Table 5.1.*

TABLE 5.1

Number of Elements	Computing Time (Sec.)
4 x 4 x 2	13
5 x 5 x 2	30
6 x 6 x 2	64
7 x 7 x 2	128

5.2.2 Effect of Numerical Correction on Thick Wing

Table 5.2 shows the comparison between the results of the tangent plane approximation and that with numerical correction for a wing with thickness ratio $\tau = .2$. The other data are the same as those for Fig. 5. The computer time

*Advantage of symmetry with respect to Z was taken.

required for both solutions are also shown. It is seen that even for this thick wing, the tangent plane approximation yields good results and considerable computer time is saved. So all the discussion given in the following subsections is based on results from this tangent plane approximation.

TABLE 5.2

	T.P.A.	T.P.A. + N.I.
C_{l_α} at root	8.09 2.60 .975	7.91 2.59 .900
Computer Time (sec)	22	136

5.2.3 Thickness Effect

In order to analyze the thickness effect, the problem has been solved for four values of the thickness ratio, τ = .1, .01, .001 and .0001, respectively. In all these cases, the number of elements in both x and y directions is NX = NY = 4. Hence, the total number of elements (for upper and lower side of the right half of the wing) is N = 32 (i.e., Eq. 4.13 is a system of 32 equations and 32 unknowns).

For the value $\tau = .001$, no message indicating strong elimination of figures was given, whereas, for the value $\tau = .0001$, a message indicating an elimination of significant figures higher than the prescribed tolerance at the 19th step was obtained.*

Hence, only the cases $\tau = .1$, $.01$, and $.001$ are presented here. The lift distribution $C_\ell = -\Delta C_p$ at the root elements, is shown in Fig. 8. The results indicate that the solution converges to a zero-thickness solution and that the solution for $\tau = .001$ is a good approximation for the zero thickness solution. It may be noted that the results here showed that a thinner wing yields a higher lift.

Note that, according to Eq. (3.6),

$$\sum_{i=1}^{N} C_{ki} = \frac{1}{2\pi} \sum_{i=1}^{N} \iint_{\Sigma_i} \frac{\partial}{\partial N_i} \left(\frac{1}{R_k}\right) d\Sigma_i = -\frac{1}{2\pi} \oint\!\!\oint_{\Sigma} d\Omega = -1 \qquad (5.2)$$

since the point from which the solid angle is evaluated is <u>on</u> the surface Σ. This equation is poorly satisfied on the leading edge and the tip where the approximation of the surface element with its tangent plane is poorer. The

---

*For the solution of Eq. (4.13), the standard IBM SUBROUTINE GELG has been used. The value of the tolerance (which is compared to the ratio between the pivot at the nth step and the initial step) was chosen to be TOL = .001.

poorest values of $\sum_{i=1}^{N} C_{ki}$ at tip or leading-edge elements", are given in Table 5.3, column 1, whereas the poorer value for the "internal element" (not at the leading edge nor at the tip) are given in column 2.

TABLE 5.3

τ	1	2
.1	.76946	.98986
.01	.96247	.99899
.001	.99625	.99990
.0001	.99960	.99999

Table 5.3 indicates that, for the case τ = .1, the approximation of the surface elements with its tangent plane is not satisfactory for the "non-internal elements".

5.3 Comparison with Existing Results

In order to evaluate the accuracy, comparisons with existing results are given in Figs. 9 to 14. Different values of Mach number, aspect ratio and different planforms are tested to show the flexibility of the program. Thickness

ratio shown in the figures are chosen arbitrarily. $\bar{\xi}$ and $\bar{\eta}$ are defined as

$$\bar{\xi} = \bar{x} / c(\eta)$$
$$\bar{\eta} = 2\bar{y} / b \qquad (5.3)$$

Figure 9 shows the comparison of the value C_ℓ between the present solution and Cunningham's Theory[11] and experiment[12] on three cross sections of a rectangular wing. As can be seen, agreement between the two theories is very good and agreement between theory and experiment is very good except when near the leading edge. Figure 10 compares the results obtained with the present method and those obtained by Hsu (Ref. 13), Kulakowski and Haskell (Ref. 14) and Cunningham (Ref. 11), for a rectangular wing of aspect ratio $\mathcal{AR} = 1$, thickness ratio $\tau = .001$ and Mach number M = .2. It may be noted the excellent agreement between the present method and the ones of Refs. 11 and 14, which are generally considered to be very accurate.

The results for a delta wing ($\mathcal{AR} = 2.5$, $\tau = .005$ and M = 0) are compared in Figure 11 with the Widnall results (see Fig. 7.7 in Ref. 15). The results for a tapered swept wing ($\mathcal{AR} = 3.0$, taper ratio = .5, $\Lambda_{\frac{1}{4}} = 45°$, M = 0.8, and $\alpha = 4.13°$) are compared in Fig. 12 with Cunningham's results (Ref. 11).

Finally, it should be noted that the comparison of the integrated values of the pressure is generally more significant than the comparison of the pressure distribution because small (relative) errors on the pressure distribution near the leading edge can yield large errors on the integrated

values. Hence, the values of the section lift coefficients

$$C_{L_\alpha} = -\int_0^1 \Delta C_{p_\alpha}\, d\xi \qquad (5.4)$$

are compared in Figs. 13, 14 and 15 to the ones obtained by Yates (Ref. 16) for a rectangular wing with aspect ratio $\mathcal{R}$ = 4,4,8, thickness ratio τ = .001 and Mach number M = 0, .507, 0, respectively. It may be noted that the Figs. 13 and 14 (incompressible and compressible flow, respectively) show an excellent agreement, whereas in Fig. 15, the agreement is less satisfactory.

In conclusion, the agreement is excellent for the cases presented in Figs. 9, 10, 13, and 14, but less satisfactory in Figs. 11, 12 and 15. The reasons for the small disagreements shown in Figs. 11, 12 and 15 are now being analyzed.

SECTION 6

CONCLUDING REMARKS

A general method for analyzing steady subsonic flow around lifting bodies of arbitrary configuration is presented in the preceeding Sections. The method is then applied to thin wings in steady compressible flow, which is the most challenging problem for this method. The results indicate that the method is accurate and does not require excessive computer time. The rate of convergence is surprisingly high. Similar results were obtained for oscillating wings in subsonic flow (Ref. 18).

Since the problem of elimination of significant figures is not encountered even for very thin wings (thickness ratio τ = .1%) it is expected that no such problems will be encountered in applying the method to realistic complex configurations. Extensions of the method to complex configurations are now under consideration.

REFERENCES

1. Garrick, I.E., "Nonsteady Wing Characteristics", High Speed Aerodynamics and Jet Propulsion",Vol. 7, Section F, Princeton University Press, 1957.
2. Ashley, H., Widnall, S., and Landahl, M.T., "New Directions in Lifting Surface Theory", AIAA J., Vol. 3, No. 1, Jan. 1965, pp. 3-16.
3. Landahl, M.T. and Stark, V.J.E., "Numerical Lifting-Surface Theory -- Problems and Progress", AIAA J., Vol. 6, No. 11, Nov. 1968, pp. 2049-2060.
4. Albano, E. and Rodden, W.P., "A Doublet-Lattice Method for Calculating Lift Distribution on Oscillating Surfaces in Subsonic Flows", AIAA J., Vol. 7, No. 2, Feb. 1969, pp. 279-285.
5. Ashley, H., and Rodden, W.P., "Wing-Body Aerodynamic Interaction", Annual Review of Fluid Mechanics, Vol. 4, 1972, pp. 431-472.
6. Morino, L., "A General Theory of Unsteady Compressible Potential Aerodynamics" NASA CR-2464, 1974 (Supersedes Boston University, Department of Aerospace Engineering, TR-72-01, 1972).
7. Chiuchiolo, E.A., "Steady Incompressible Potential Flow Around Lifting Bodies Immersed in a Fluid", Boston Univ., Department of Aerospace Engineering, Master Thesis, 1974.
8. Greenberg, M.D., Application of Green's Functions in Science and Engineering, Prentice-Hall, 1971.

9. Smirnov, A.I., A Course of Higher Mathematics, Vol. 4, Addison-Wesley, 1964.

10. Djojodihardjo, R.H. and Widnall, W.E., "A Numerical Method for the Calculation of Nonlinear Unsteady Lifting Potential Flow Problems", AIAA J., Vol. 7, No. 10, Oct. 1969, pp. 2001-2009.

11. Cunningham, A.M. Jr., "An Efficient, Steady Subsonic Collocation Method for Solving Lifting-Surface Problems", J. Aircraft, Vol. 8, No. 3, March 1971, pp. 168-176.

12. Lessing, H.C., Troutman, J.C. and Menees, G.P., "Experimental Determination of the Pressure Distribution on a Rectangular Wing Oscillating in the First Bending Mode for Mach Numbers from 0.24 to 1.30", NASA TN D-344, 1960.

13. Hsu, P.T., "Flutter of Low Aspect-Ratio Wings, Part I, Calculation of Pressure Distributions for Oscillating Wings of Arbitrary Platform in Subsonic Flow by the Kernel-Function Methods", TR-64-1, October 1957, M.I.T.

14. Kulakowski, L.J. and Haskell, R.N., "Solution of Subsonic Nonplanar Lifting Surface Problems by Means of High-Speed Digital Computers", Journal of Aerospace Sciences, Vol. 28, February 1961, pp. 103-113.

15. Ashley, H. and Landahl, M., Aerodynamics of Wings and Bodies, Addison-Wesley Pub. Co., Inc., 1965, pp. 159.

16. Kolbe, C.D. and Boltz, F.W., "The Forces and Pressure Distribution at Subsonic Speeds on a Planar Wing Having 45° of Sweep Back, an Aspect Ratio of 3, and a Taper Ratio of 0.5", RMA51G31, October 1951, NACA.

17. Yates, E.C. Jr., "Flutter Prediction at Low Mass-Density Ratios with Application to the Finite-Span Noncavitating Hydrofoil", AIAA Paper No. 68-472, San Diego, Calif., April-May 1968.

18. Morino, L. and Kuo, C.C., "Unsteady Subsonic Flow Around Oscillating Finite-Thickness Wings", Boston University, Department of Aerospace Engineering, TR-73-03, February 1973.

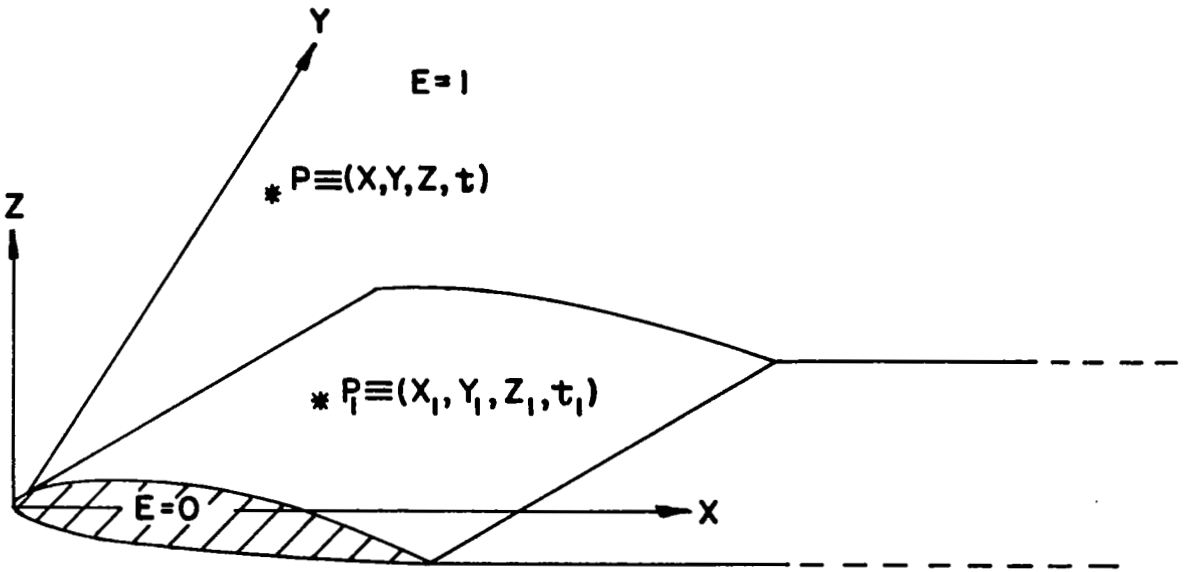

Fig. 1 Geometry of the problem

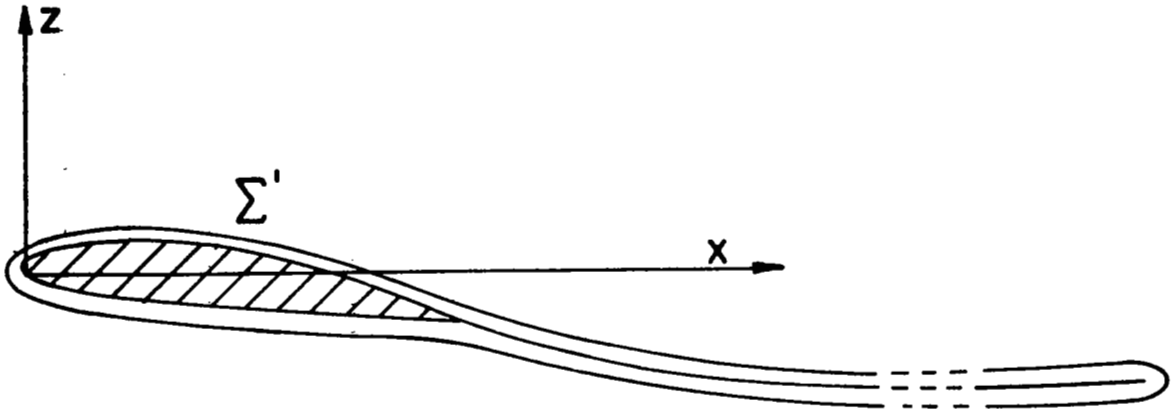

Fig. 2a The surface Σ'

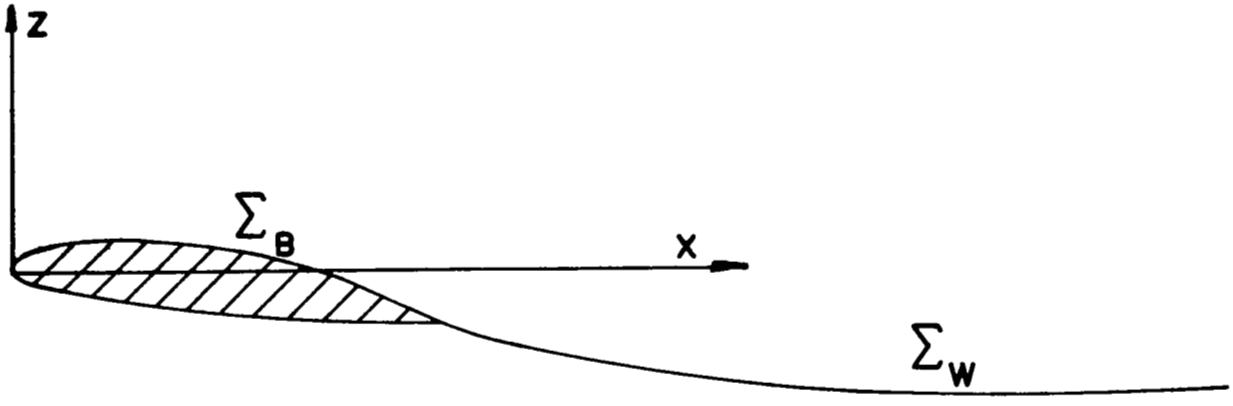

Fig. 2b The surfaces Σ_B and Σ_W

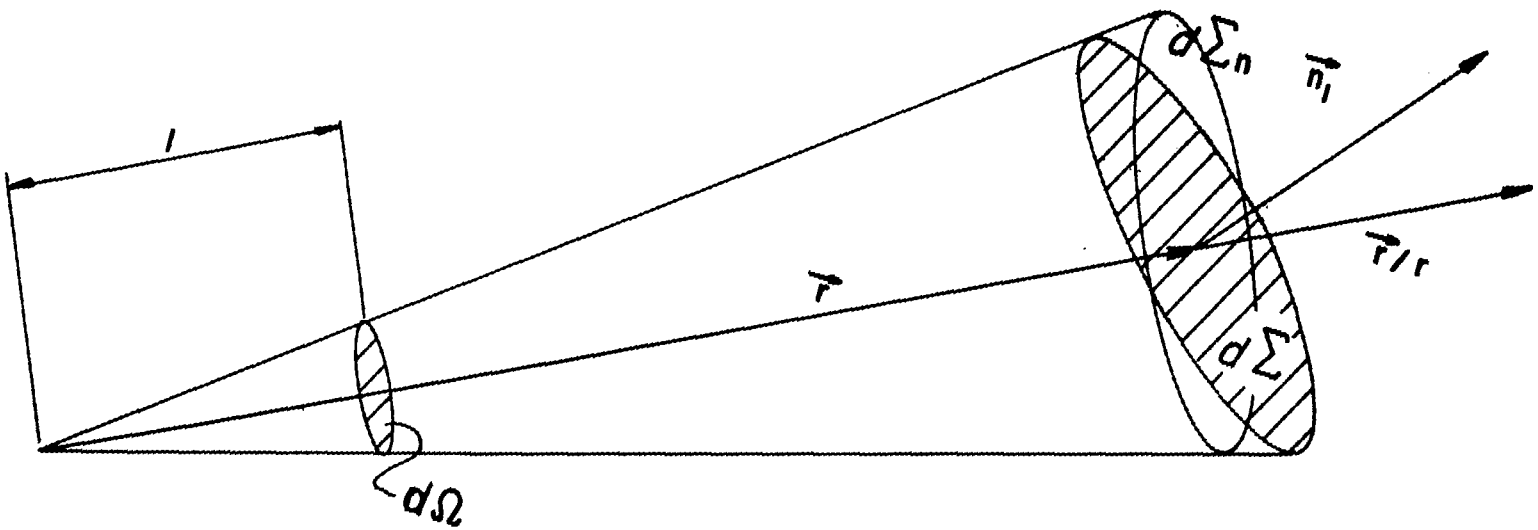

Fig. 3 Solid angle Ω

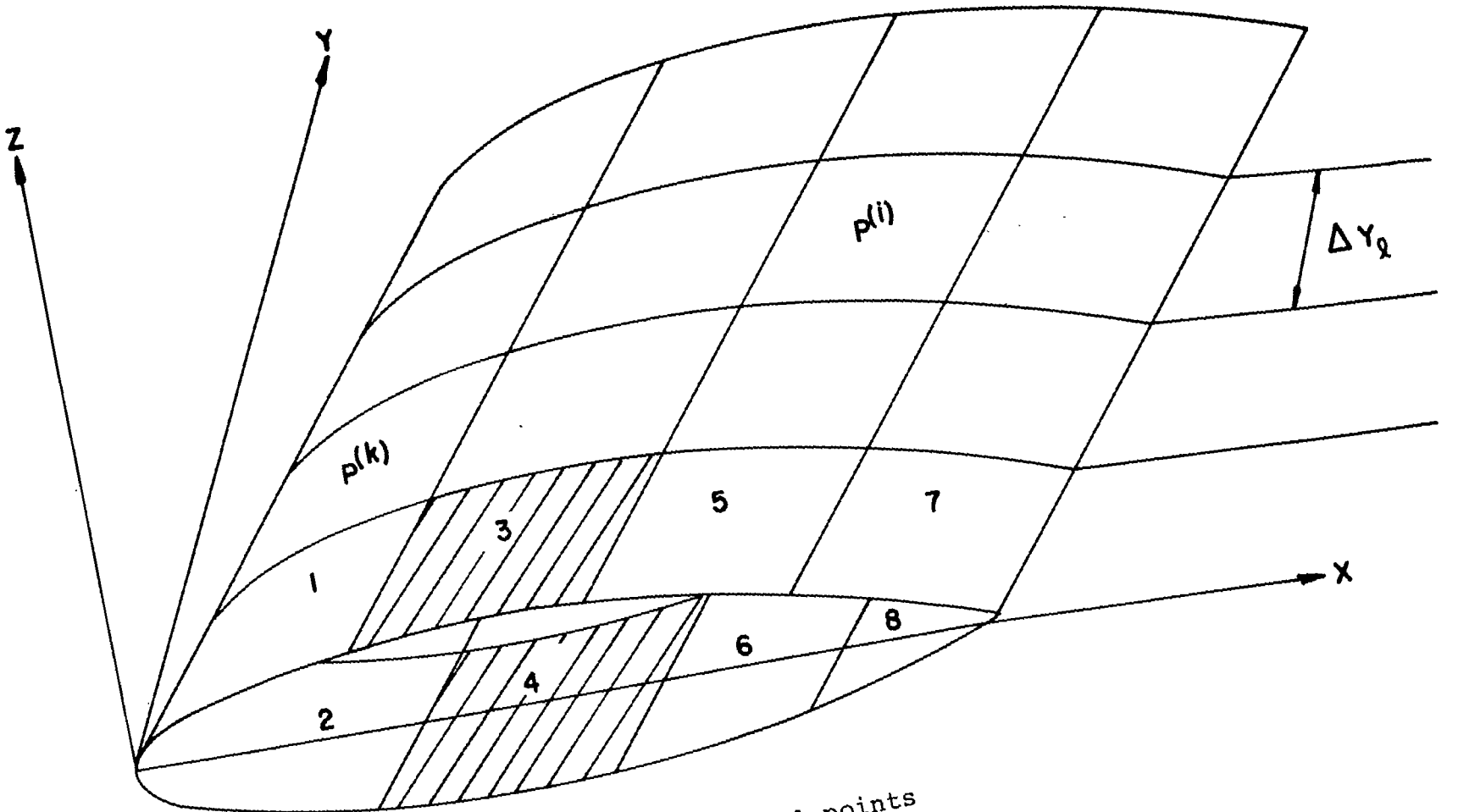

Fig. 4 Elements and control points

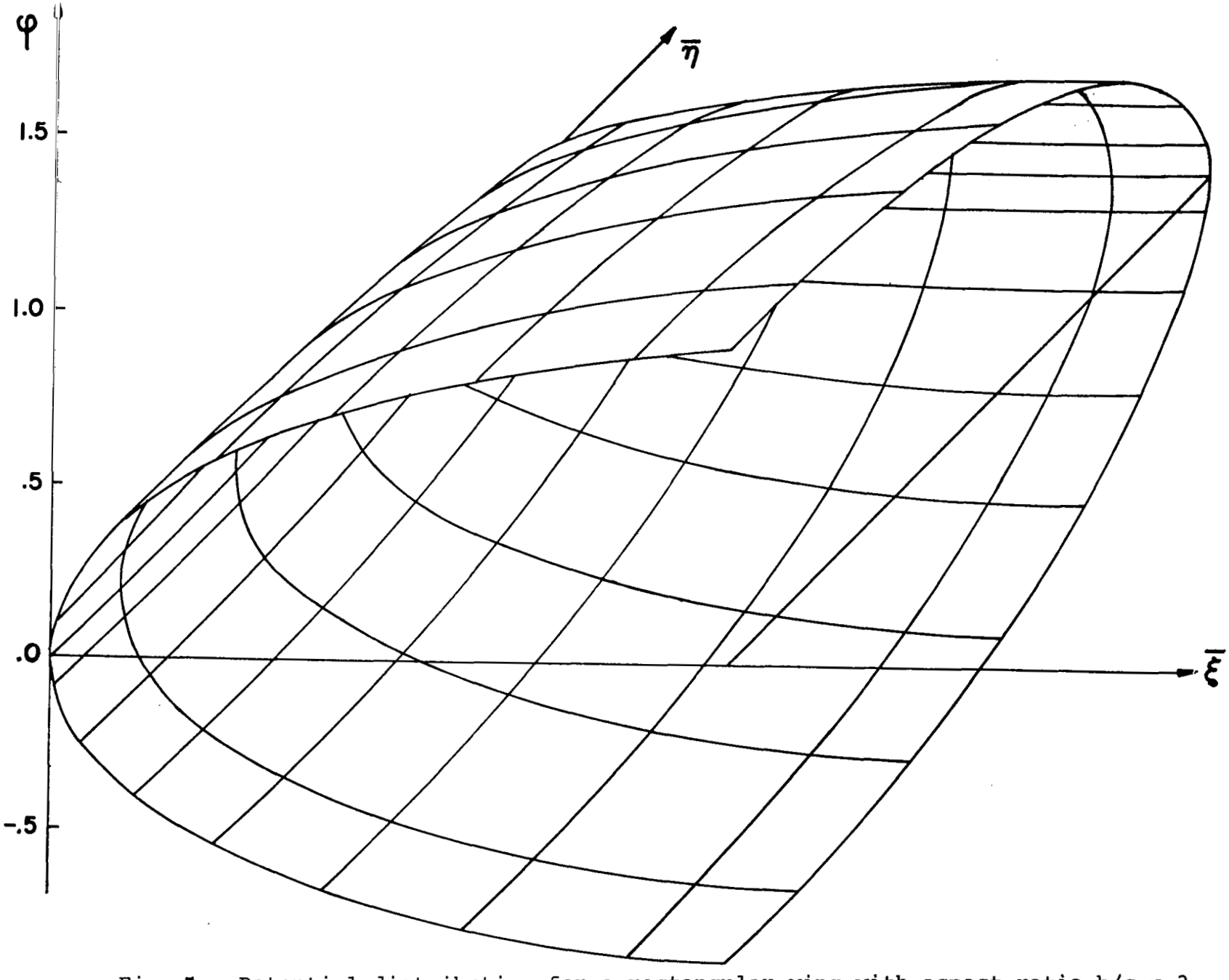

Fig. 5 Potential distribution for a rectangular wing with aspect ratio b/c = 3, angle of attack α = 5° and Mach number M = .24

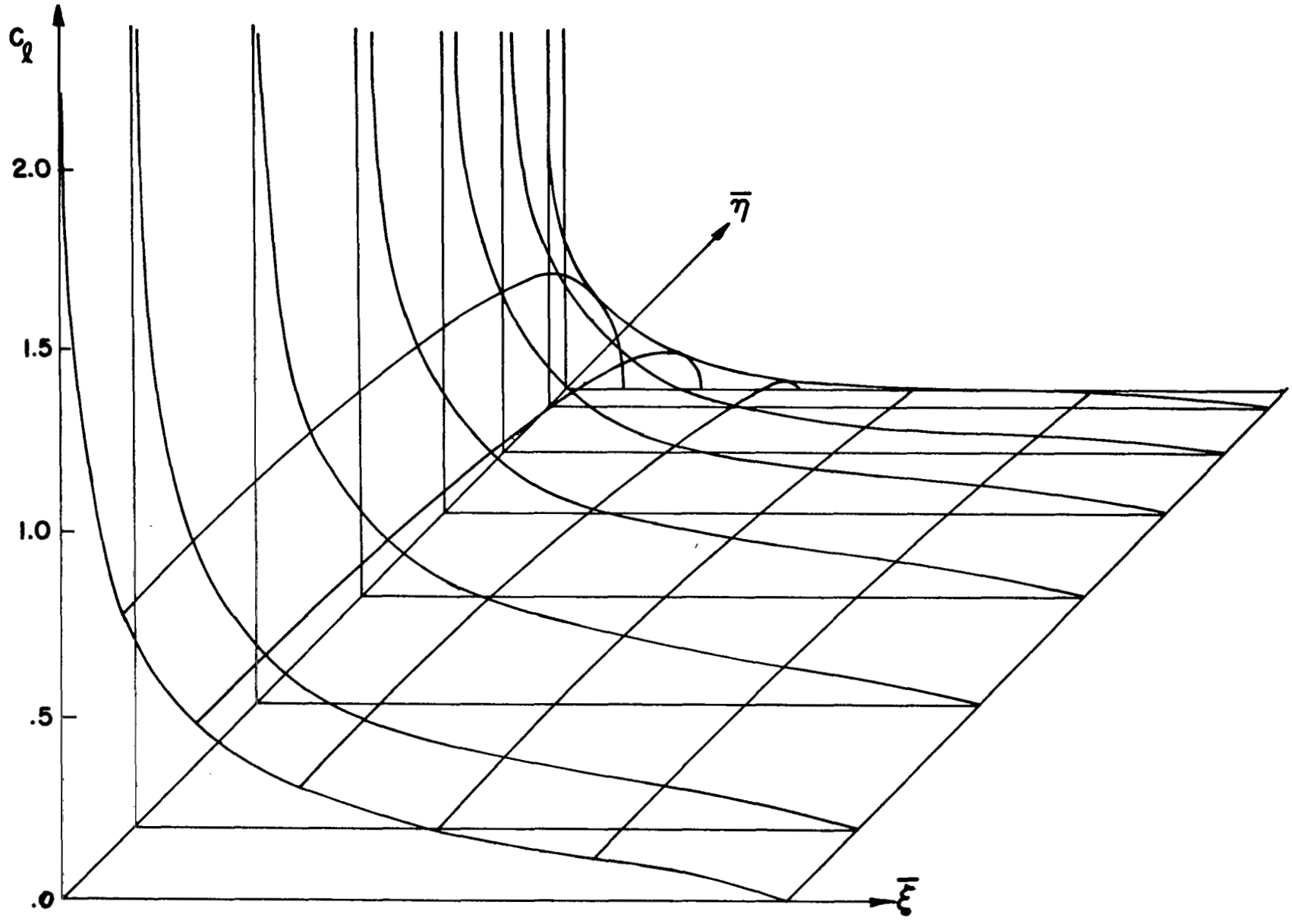

Fig. 6 Lifting pressure distribution for a rectangular wing with aspect ratio b/c = 3, angle of attack α = 5° and Mach number M = .24

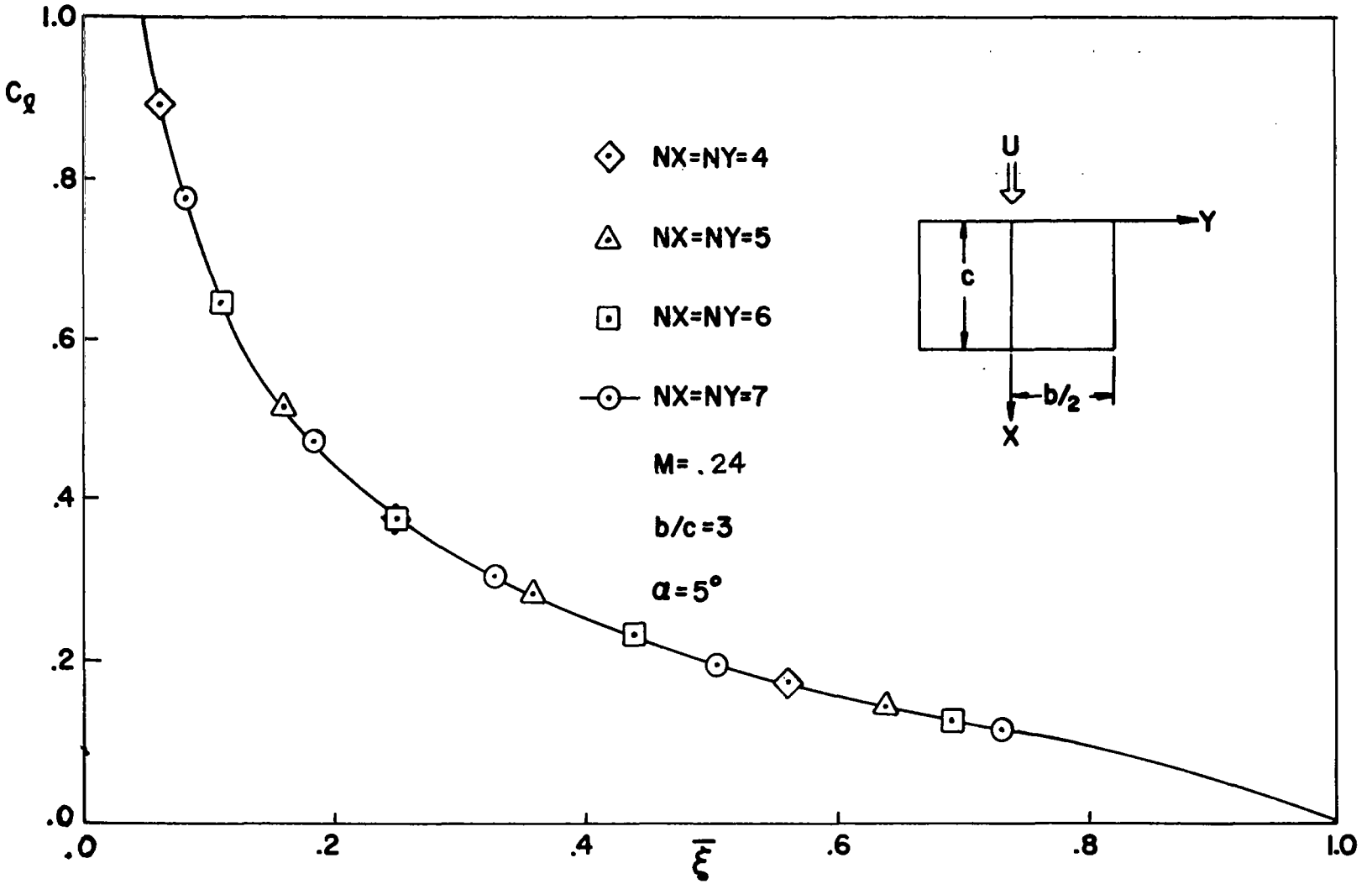

Fig. 7 Lifting pressure coefficient at root boxes for thickness ratio τ = .001 and different values of NX and NY for a rectangular wing with aspect ratio b/c = 3, angle of attack α= 5° and Mach number M = .24

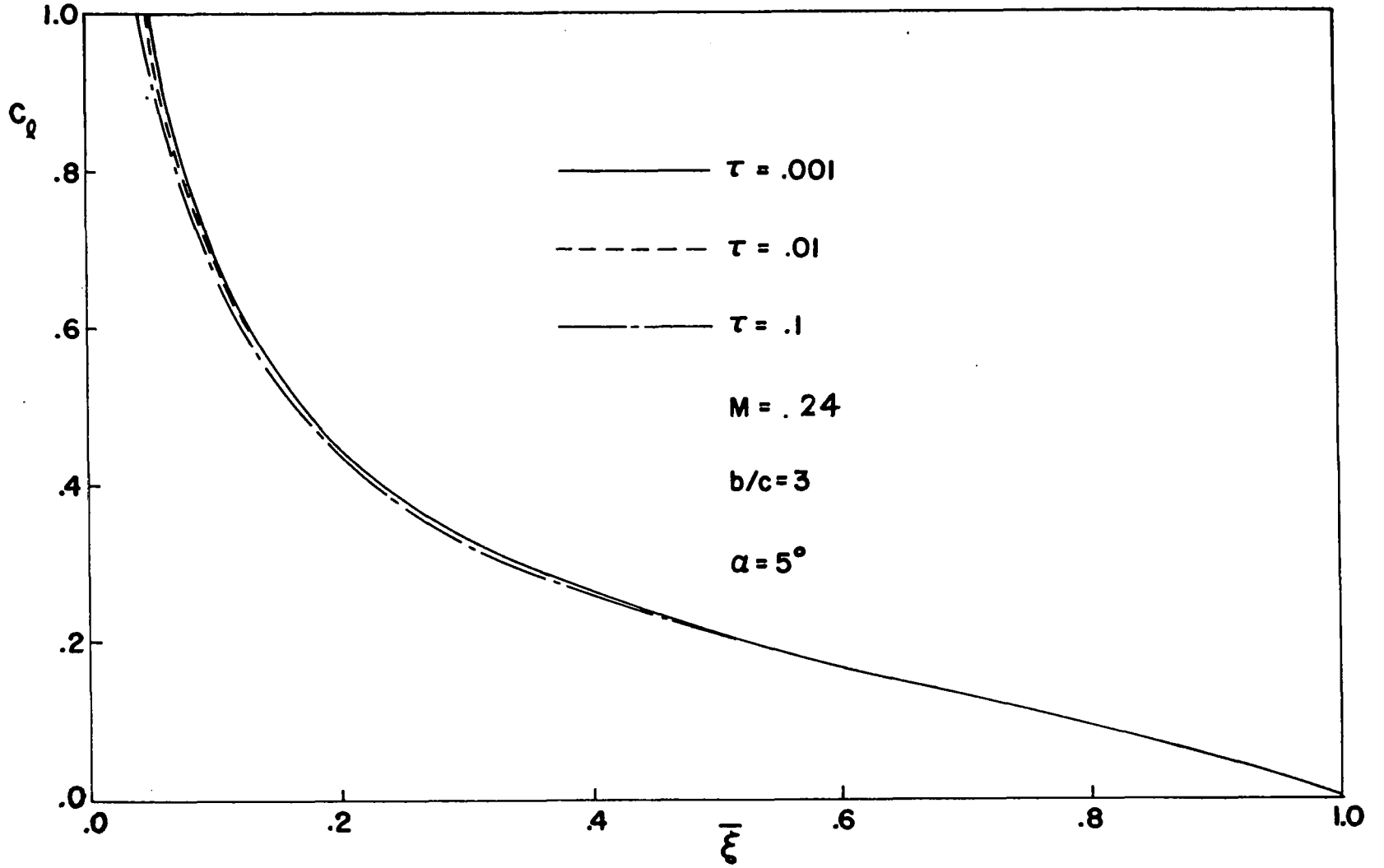

Fig. 8 Effect of decreasing thickness on the numerical scheme: Lifting pressure coefficient at the root boxes for NX = NY = 4 and different values of the thickness ratio τ , for a rectangular wing with aspect ratio b/c = 3, angle of attack α = 5° and Mach number M = .24

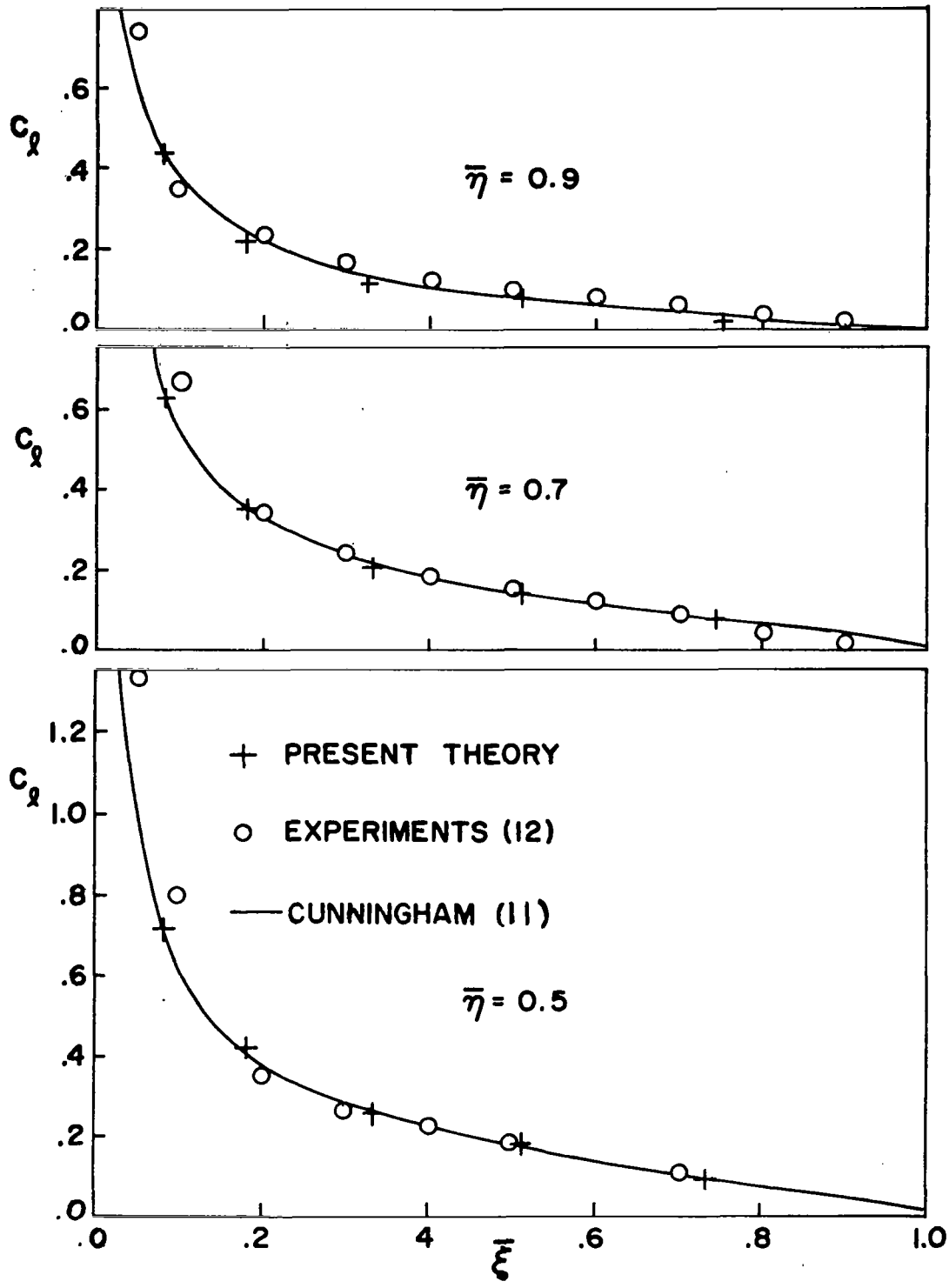

Fig. 9 Lift distribution for a rectangular wing with aspect ratio b/c = 3, angle of attack α = 5° and Mach number M = .24

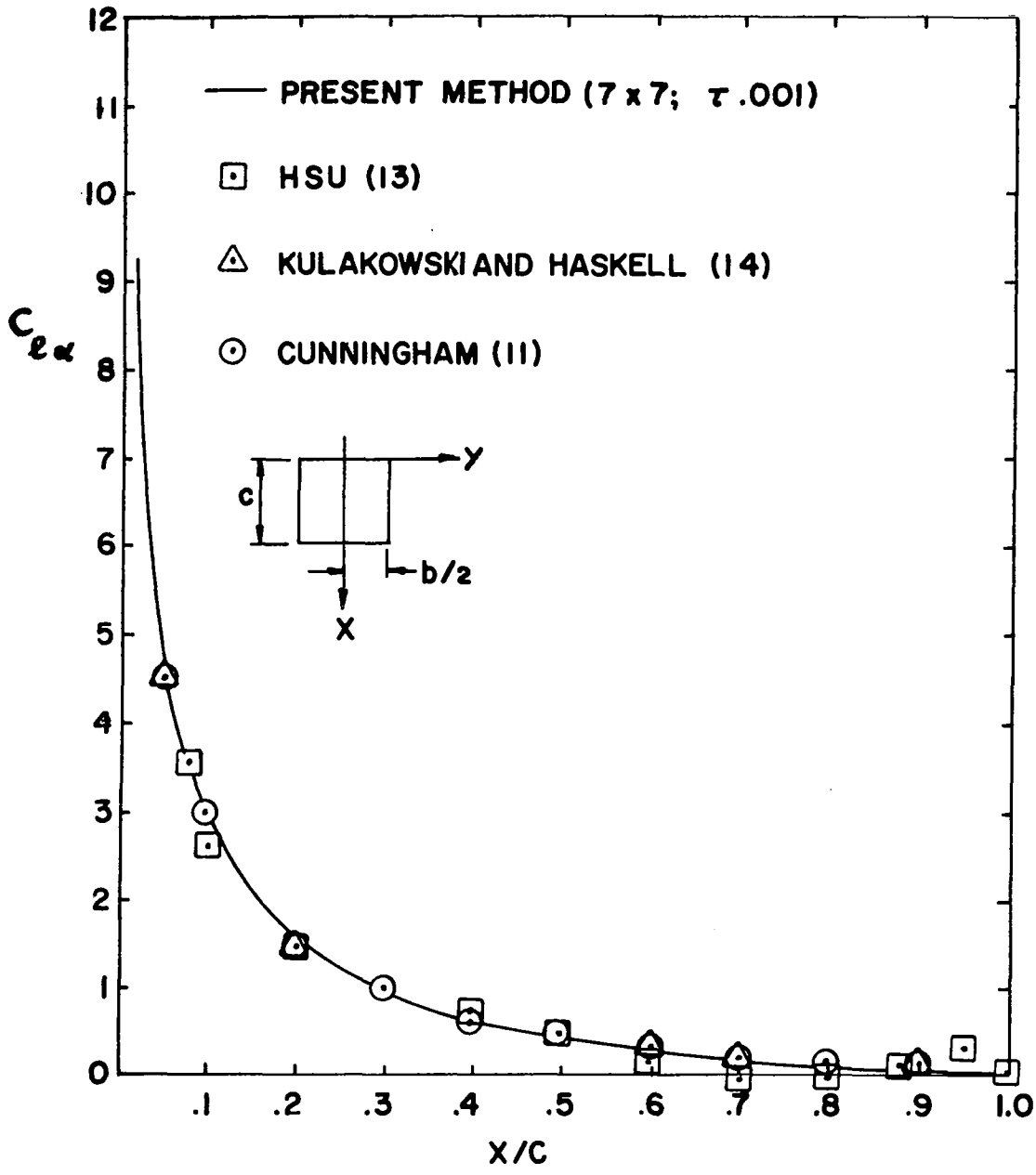

Fig. 10 Lift distribution per unit angle of attack at 2y/b = .7 for a rectangular wing with aspect ratio A.R. = 1 and Mach number M = .2

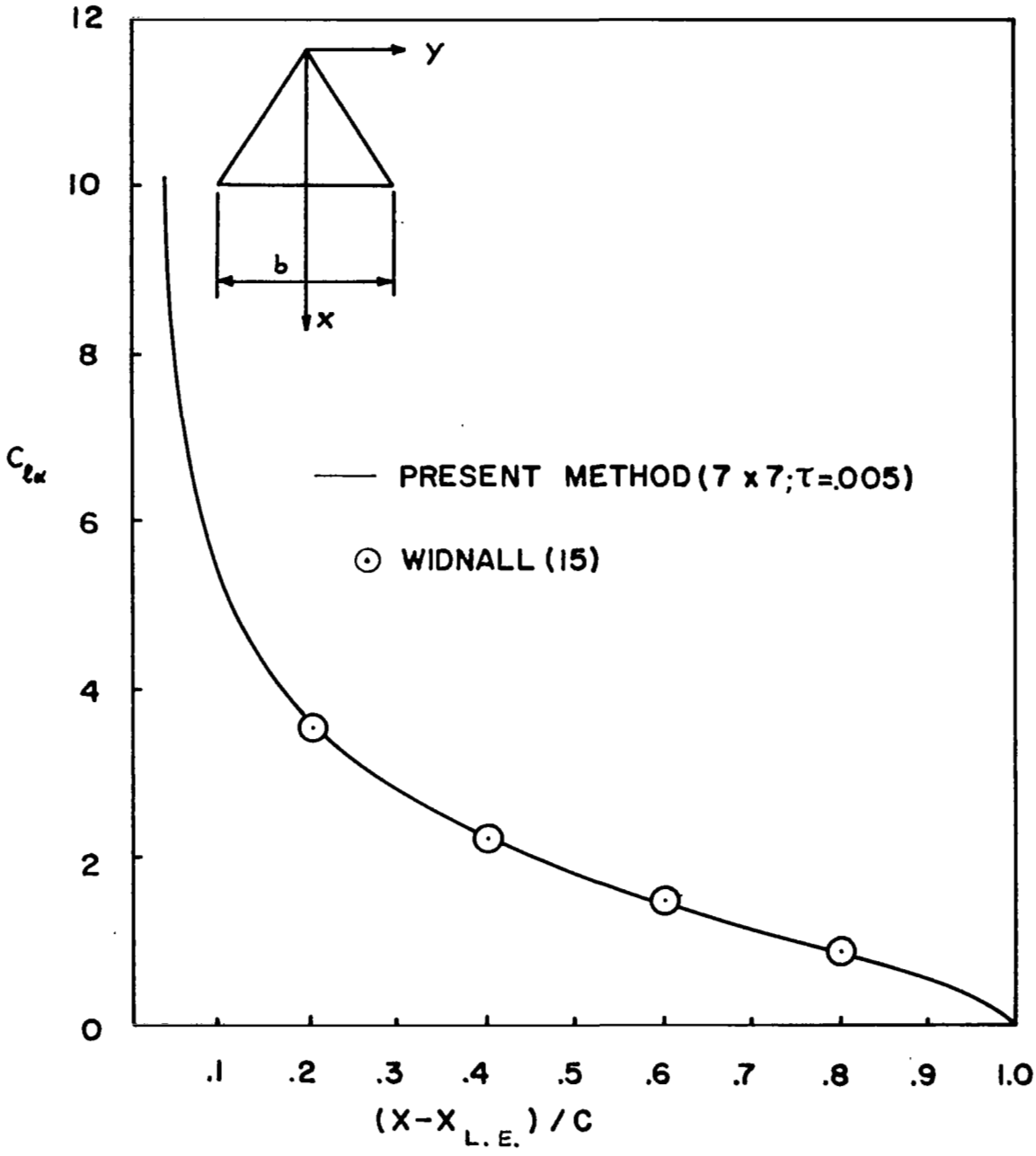

Fig. 11 Lift distribution per unit angle of attack at 2y/b = .5 for delta wing with aspect ratio A.R. = 2.5, and Mach number M = 0

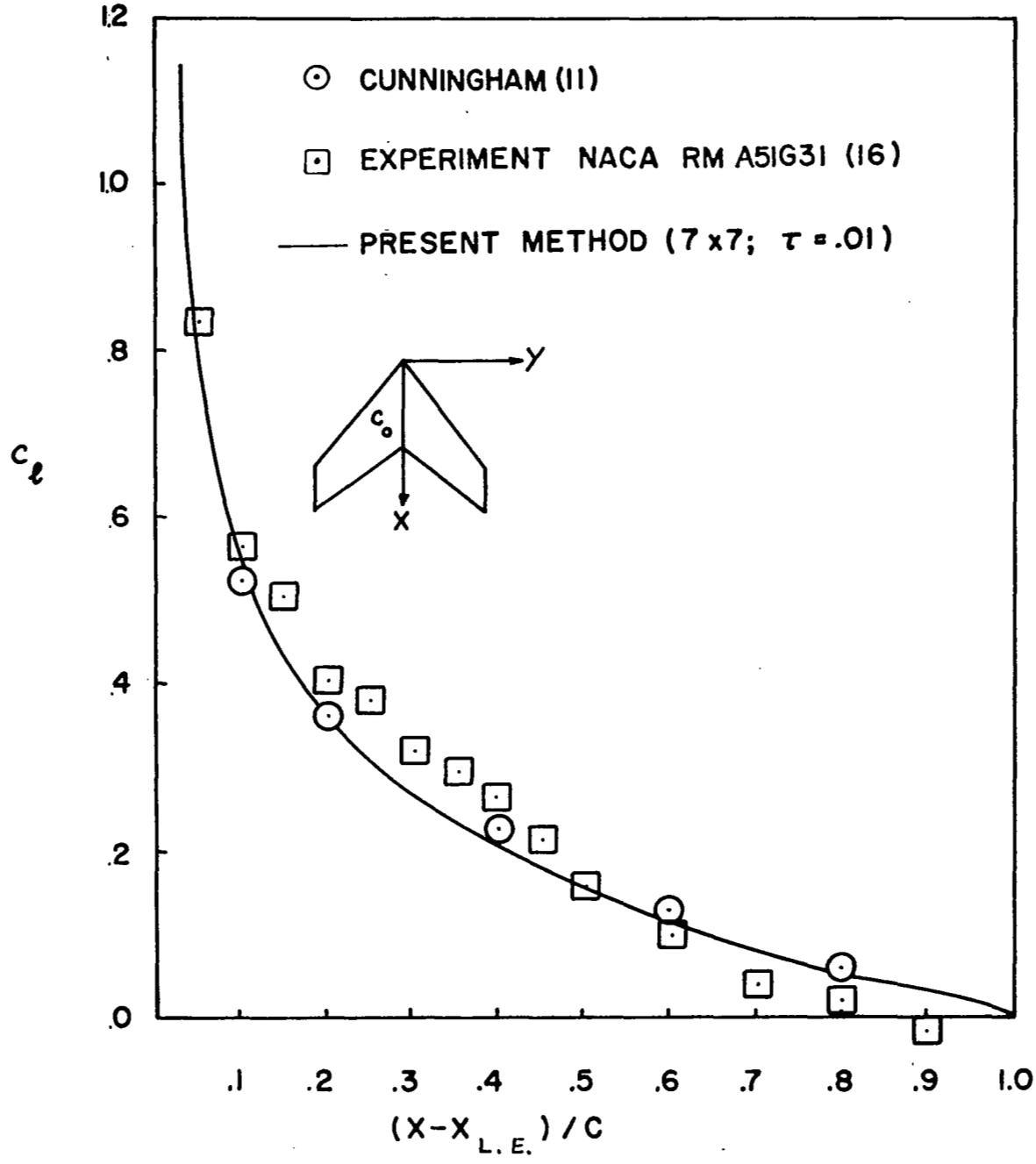

Fig. 12 Lift Distribution at 2y/b = .707 for a swept tapered wing with aspect ratio A.R. = 3, taper ratio T.R. = .5, $\Lambda_{1/4}$ = 45°, angle of attack α = 4.13°, and Mach number M = .8

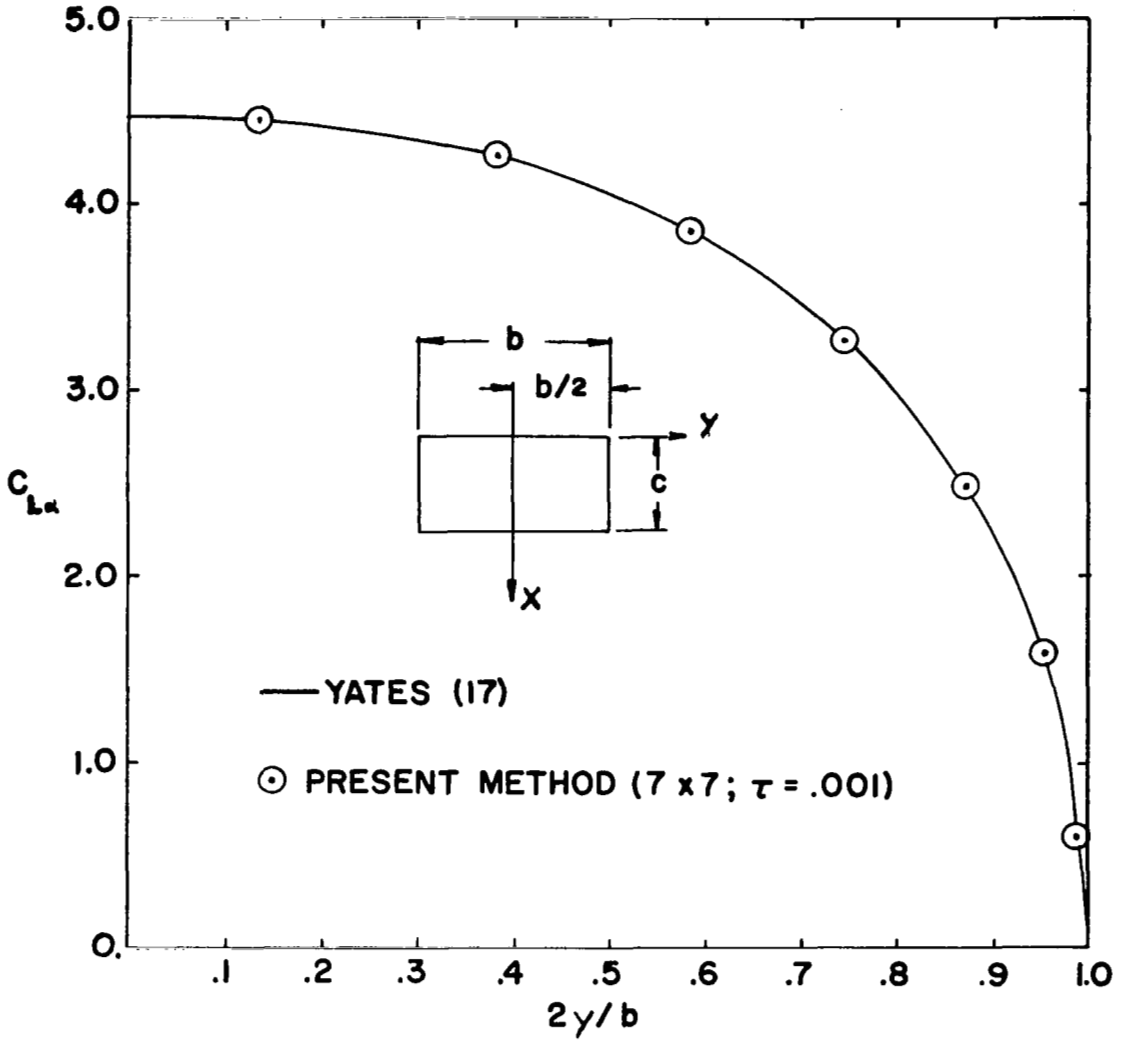

Fig. 13 Section lift-curve slope for rectangular wing with aspect ratio A.R. = 4 and Mach number M = 0

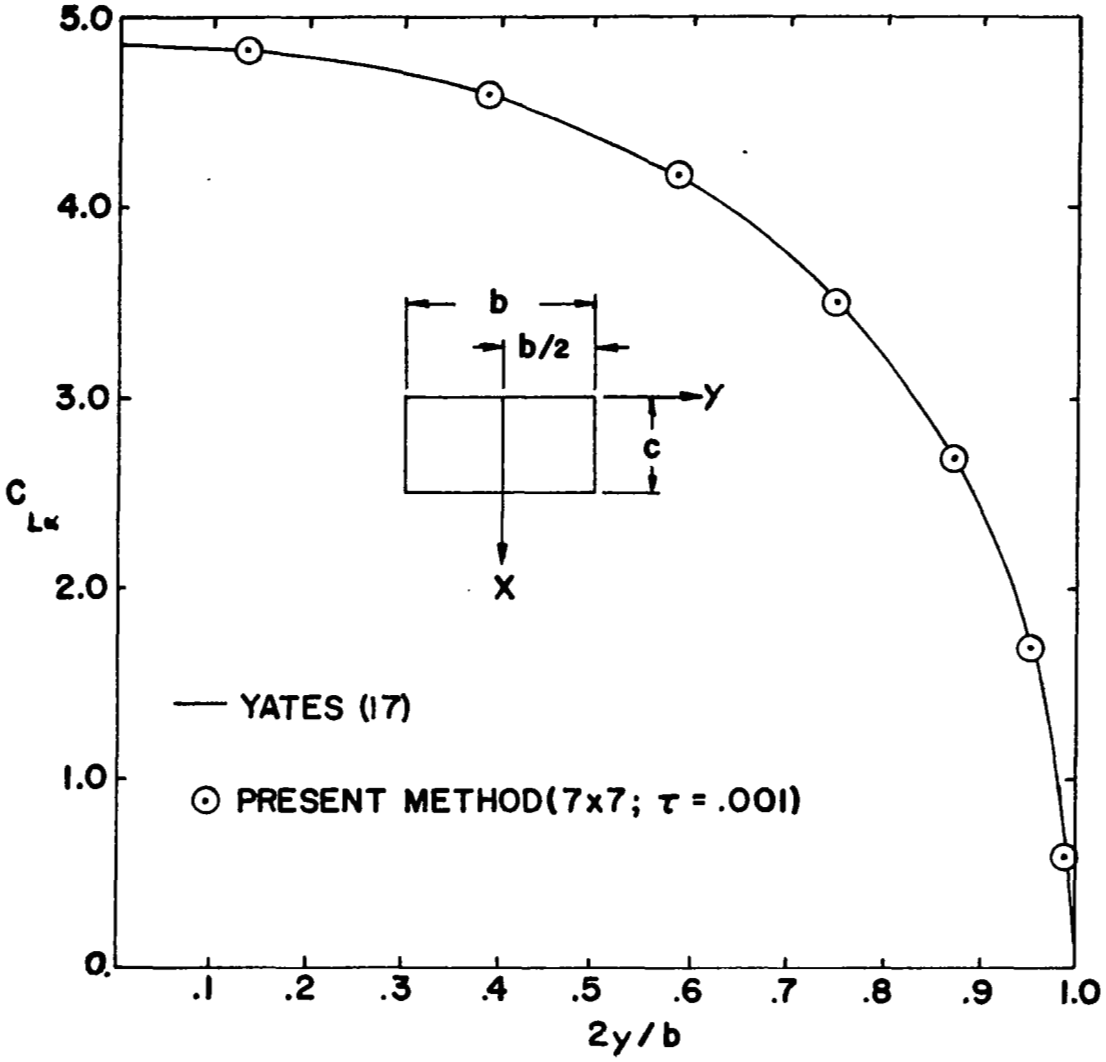

Fig. 14 Section lift-curve slope for rectangular wing with aspect ratio A.R. = 4 and Mach number M = .507

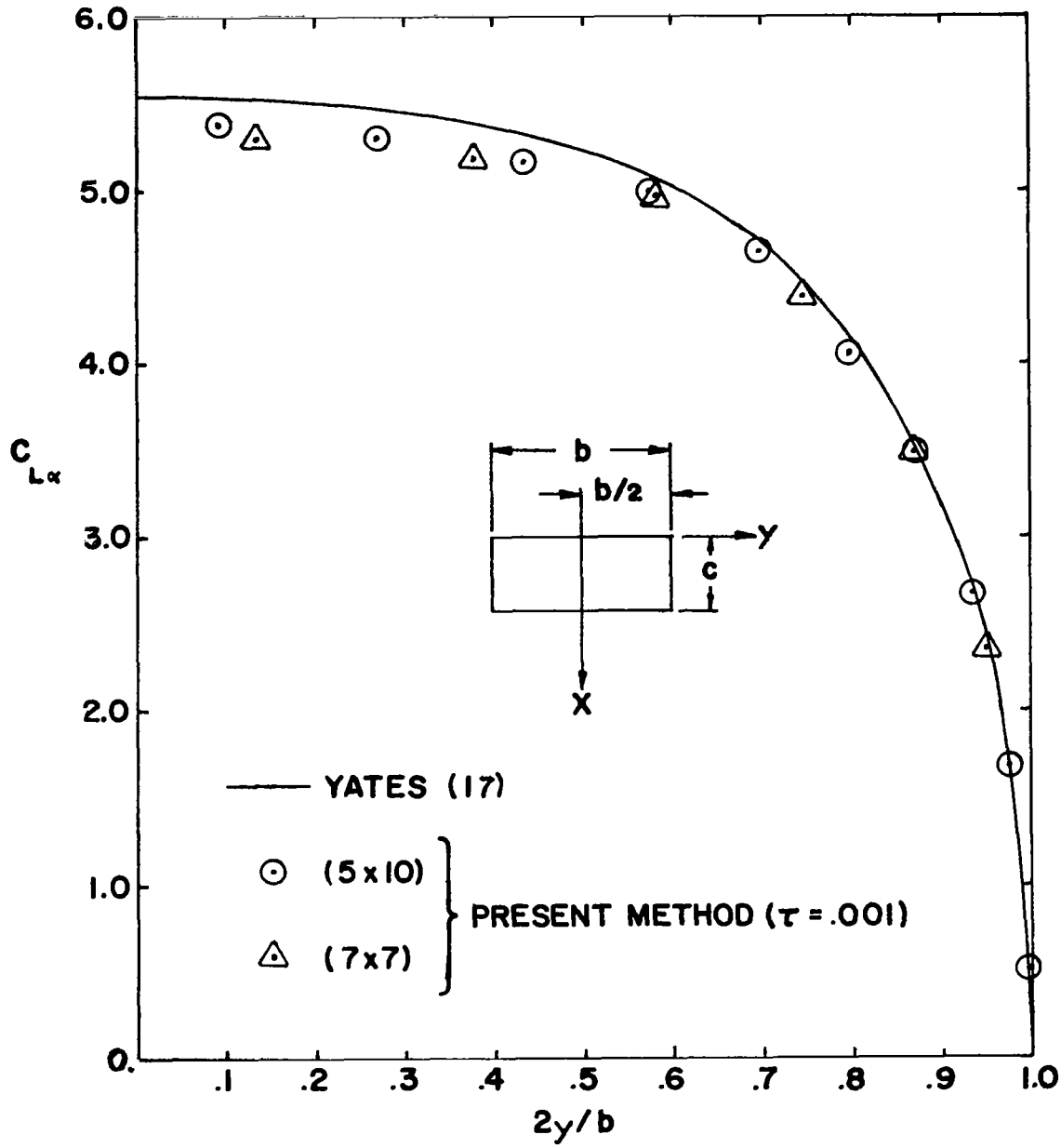

Fig. 15 Section lift-curve slope for rectangular wing with aspect ratio A.R. = 8 and Mach number M = 0

APPENDIX A

THE VALUE OF THE FUNCTION E ON THE SURFACE

A.1 Introduction

Equation (2.19) gives a representation of the potential anywhere in the volume, in terms of the values of $\partial\varphi/\partial n$ and φ on the surface of the body. The values of $\partial\varphi/\partial n$ on the surface of the body are given by the boundary conditions, but the values of φ are not known. In order to solve the problem, it is thus necessary to obtain first the values of φ on the surface. This can be done by letting the point P of the volume V approach a point P_* of the surface.

In this Appendix, it is shown that, in the limit, Eq. (2.19) is still valid if the definition of the function E is generalized as follows

$$\begin{aligned} E &= 1 \quad \text{outside } \Sigma \\ E &= 1/2 \quad \text{on } \Sigma \\ E &= 0 \quad \text{inside } \Sigma \end{aligned} \tag{A.1}$$

By letting $P \to P_*$, the integrands become singular in the neighborhood of P_*. Thus, it is convenient to separate the contribution of a small neighborhood* of P_*, which will be indicated as Σ_ϵ.

For steady compressible flow, Eq. (2.19) can be rewritten

---

*The neighborhood Σ_ϵ is a small circular surface element, with center P_* and radius ϵ.

as

$$4\pi E\varphi = -\iint_{\Sigma-\Sigma_\epsilon} \frac{\partial\varphi}{\partial N_1}\frac{1}{R}d\Sigma + \iint_{\Sigma-\Sigma_\epsilon} \varphi\frac{\partial}{\partial N_1}\left(\frac{1}{R}\right)d\Sigma + \delta_\epsilon \qquad (A.2)$$

where δ_ϵ is the contribution of the neighborhood of P_*, given by

$$\delta_\epsilon = -\iint_{\Sigma_\epsilon} \frac{\partial\varphi}{\partial n_1}\frac{1}{R}d\Sigma + \iint_{\Sigma_\epsilon} \varphi\frac{\partial}{\partial N_1}\left(\frac{1}{R}\right)d\Sigma \qquad (A.3)$$

The analysis of δ_ϵ is highly simplified by using local coordinate $\hat{X}$, $\hat{Y}$, $\hat{Z}$, with $\hat{Z}$ normal to the tangent plane (directed from E = 0 to E = 1). Then, separating terms of order ϵ, Eq. (A.3) reduces to*

$$\delta_\epsilon = -\left(\frac{\partial\varphi}{\partial\hat{Z}_1}\right)_* \iint_{\hat{X}_1^2+\hat{Y}_1^2\le\epsilon^2} \frac{1}{\sqrt{\hat{X}_1^2+\hat{Y}_1^2+\hat{Z}^2}}\,d\hat{X}_1\,d\hat{Y}_1 \qquad (A.4)$$

$$-\varphi_* \iint_{\hat{X}_1^2+\hat{Y}_1^2\le\epsilon^2} \frac{\partial}{\partial\hat{Z}}\frac{1}{\sqrt{\hat{X}_1^2+\hat{Y}_1^2+\hat{Z}^2}}\,d\hat{X}_1\,d\hat{Y}_1 + O(\epsilon)$$

where the subscript * indicates evaluation at P_*. By using polar coordinate

$$\hat{R} = \sqrt{\hat{X}_1^2+\hat{Y}_1^2} \qquad (A.5)$$
$$\hat{\theta} = \tan^{-1}\hat{Y}_1/\hat{X}_1$$

one obtains

---

*Note that $\hat{X} = \hat{Y} = 0$, $\hat{Z}_1 = 0$ and $\partial/\partial\hat{Z}_1\,|_{\hat{Z}_1=0} = -\partial/\partial\hat{Z}\,|_{\hat{Z}_1=0}$

$$\delta_\epsilon = -2\pi \left(\frac{\partial \varphi}{\partial \hat{Z}_1}\right)_* \int_0^\epsilon \frac{1}{\sqrt{\hat{R}^2+\hat{Z}^2}}\, \hat{R}\, d\hat{R}$$

$$-2\pi \varphi_* \int_0^\epsilon \frac{\partial}{\partial \hat{Z}} \frac{1}{\sqrt{\hat{R}^2+\hat{Z}^2}}\, \hat{R}\, d\hat{R} + O(\epsilon) \qquad \text{(A.6)}$$

Noting that

$$\frac{1}{\hat{Z}} \frac{\partial}{\partial \hat{Z}} \left(\frac{1}{\sqrt{\hat{R}^2+\hat{Z}^2}}\right) = -\left(\hat{R}^2+\hat{Z}^2\right)^{-3/2} = \frac{1}{\hat{R}} \frac{\partial}{\partial \hat{R}} \left(\frac{1}{\sqrt{\hat{R}^2+\hat{Z}^2}}\right) \qquad \text{(A.7)}$$

Eq. (A.6) becomes

$$\delta_\epsilon = -2\pi \left(\frac{\partial \varphi}{\partial \hat{Z}}\right)_* \left[\sqrt{\hat{R}^2+\hat{Z}^2}\right]_0^\epsilon$$

$$-2\pi \varphi_* \hat{Z} \left[\frac{1}{\sqrt{\hat{R}^2+\hat{Z}^2}}\right]_0^\epsilon + O(\epsilon) \qquad \text{(A.8)}$$

Finally, by letting P go to P_*, (that is, $\hat{Z} \to 0$), one obtains

$$\lim_{P \to P_*} \delta_\epsilon = \lim_{\hat{Z} \to 0} \left[-2\pi \left(\frac{\partial \varphi}{\partial \hat{Z}_1}\right)_* \left(\sqrt{\epsilon^2+\hat{Z}^2} - |\hat{Z}|\right)\right.$$

$$\left. -2\pi \varphi_* \left(\frac{\hat{Z}}{\sqrt{\epsilon^2+\hat{Z}^2}} - \frac{\hat{Z}}{|\hat{Z}|}\right)\right] + O(\epsilon)$$

$$= \left[-2\pi \left(\frac{\partial \varphi}{\partial Z_1}\right)_* \epsilon + 2\pi \varphi_* \frac{\hat{Z}}{|\hat{Z}|}\right] + O(\epsilon) \qquad \text{(A.9)}$$

$$= \pm 2\pi \varphi_* + O(\epsilon)$$

where the upper (lower) sign holds for $Z > 0$ ($Z < 0$), that is, when P originates outside (inside) the surface Σ, correspondingly, the function E assumes the value E = 1 (E = 0).

Finally, using this result in Eq. (A.4), one obtains

$$4\pi\left(E \pm \frac{1}{2}\right)\varphi_* = -\iint_{\Sigma-\Sigma_\epsilon} \frac{\partial\varphi}{\partial N_1}\frac{1}{R}\,d\Sigma + \iint_{\Sigma-\Sigma_\epsilon} \varphi\,\frac{\partial}{\partial N_1}\frac{1}{R}\,d\Sigma + O(\epsilon) \qquad \text{(A.10)}$$

Note that, in both cases (P inside or outside Σ),

$$E_* = E \mp \frac{1}{2} = 1 - \frac{1}{2} = \frac{1}{2} \qquad \text{(A.11)}$$
$$= 0 + \frac{1}{2} = \frac{1}{2}$$

Furthermore, R_* is the distance between the dummy point, P_1, and the control point (on the surface Σ), P_*. Hence, by letting ϵ go to zero, Eq. (A.10) yields

$$4\pi E_* \varphi_* = -\oint\!\!\!\!\!\!\diagup_{\Sigma} \frac{\partial\varphi}{\partial N_1}\frac{1}{R_*}\,d\Sigma + \oint\!\!\!\!\!\!\diagup_{\Sigma} \varphi\,\frac{\partial}{\partial N_1}\left(\frac{1}{R_*}\right)d\Sigma \qquad \text{(A.12)}$$

It should be emphasized that the limit $\epsilon \to 0$ is now performed with P on the surface Σ. This implies that the contribution of Σ_ϵ is now of order ϵ. In order to clarify this point, consider the quantity

$$I_{\epsilon_0}^{\epsilon} = \int_{\epsilon_0}^{\epsilon} \frac{\partial}{\partial\hat{Z}}\left(\frac{1}{\hat{R}^2+\hat{Z}^2}\right)^{1/2}\hat{R}\,d\hat{R} \qquad \text{(A.13)}$$
$$= \left[\frac{\hat{Z}}{\sqrt{\hat{R}^2+\hat{Z}^2}}\right]_{\epsilon_0}^{\epsilon} = \frac{\hat{Z}}{\sqrt{\epsilon^2+\hat{Z}^2}} - \frac{\hat{Z}}{\sqrt{\epsilon_0^2+\hat{Z}^2}}$$

and note that

$$\lim_{\hat{Z}\to 0}\left\{\lim_{\epsilon_0\to 0} I^{\epsilon}_{\epsilon_0}\right\} = \lim_{\hat{Z}\to 0}\left\{\frac{\hat{Z}}{\sqrt{\epsilon^2+\hat{Z}^2}} - \frac{\hat{Z}}{|\hat{Z}|}\right\} = sign(\hat{Z}) \tag{A.14}$$

whereas

$$\lim_{\epsilon_0\to 0}\left\{\lim_{\hat{Z}\to 0} I^{\epsilon}_{\epsilon_0}\right\} = \lim_{\epsilon_0\to 0} 0 = 0 \tag{A.15}$$

The difference between these two limits is due to the fact that, in the limit (as $Z \to 0$), the integrand of $I^{\epsilon}_{\epsilon_0}$ behaves like a Dirac delta function and hence, its contribution for a domain which excludes the singular point is zero.

It may be worth noting that, in Eq. (A.9), the sequence of limits indicated in Eq. (A.14) must be performed, whereas in Eq. (A.12), the one indicated in Eq. (A.15) must be used.

Finally, it is shown that the results obtained here are equivalent to the definition of E given by Eq. (A.1).

Note that Eq. (2.19) must be used if P is outside or inside the surface, whereas Eq. (A.12) must be used if P is on the surface. However, by comparing Eqs. (A.12) and (2.19), it is easily seen that Eq. (2.19) is valid everywhere (outside, inside and on the surface Σ), if the convention is made that E is given by Eq. (A.1).

APPENDIX B

SOURCES AND DOUBLETS ON A TRAPEZOIDAL ELEMENT

B.1 Trapezoidal Element

In this Appendix, the effect of the sources and doublets distributed on a trapezoidal planar element, are obtained in analytic form. As mentioned in Section 4, it is of interest to consider planar elements described by the equation

$$Z_1 - Z_{1c} = \bar{\alpha}\,(X_1 - X_{1c}) + \bar{\beta}\,(Y_1 - Y_{1c}) \tag{B.1}$$

where the subscript c stands for centroid of the element, defined in Eq. (4.30). The boundary of the projection of this element on the plane $Z = 0$ is given by

$$X_{1m} + d_m(Y_1 - Y) \le X_1 \le X_{1p} + d_p(Y_1 - Y) \tag{B.2}$$

$$Y_{1m} \le Y_1 \le Y_{1p}$$

Equation (B.2) represents a trapezoid and the element defined by Eqs. (B.1) and (B.2) is called trapezoidal planar element (see Fig. B.1).

B.2 Doublet Distribution

Consider first the integral of a doublet distribution of unit density over a trapezoidal planar element, given by

$$\hat{\hat{I}}_D = \iint \frac{\partial}{\partial N_1}\left(\frac{1}{R}\right) d\Sigma \tag{B.3}$$

$$= -\int_{Y_{1m}}^{Y_{1p}} dY_1 \int_{X_{1m}+d_m(Y_1-Y)}^{X_{1p}+d_p(Y_1-Y)} \frac{1}{R^3}\left|\frac{\partial S}{\partial Z_1}\right|^{-1}\left[\frac{\partial S}{\partial X_1}(X_1-X)+\frac{\partial S}{\partial Y_1}(Y_1-Y)+\frac{\partial S}{\partial Z_1}(Z_1-Z)\right] dX_1$$

$$= S\int_{Y_{1m}}^{Y_{1p}} dY_1 \int_{X_{1m}+d_m(Y_1-Y)}^{X_{1p}+d_p(Y_1-Y)} \left[\bar{\alpha}(X_1-X)+\bar{\beta}(Y_1-Y)-(Z_1-Z)\right]\frac{1}{R^3} dX_1$$

where

$$S = \frac{\partial S/\partial Z_1}{|\partial S/\partial Z_1|} = \begin{cases} 1 & \text{on upper surface} \\ -1 & \text{on lower surface} \end{cases} \tag{B.4}$$

and use has been made of the fact that, according to Eq. (B.1),

$$\bar{\alpha} = -\frac{\partial S}{\partial X_1} \Big/ \frac{\partial S}{\partial Z_1} \tag{B.5}$$

$$\bar{\beta} = -\frac{\partial S}{\partial Y_1} \Big/ \frac{\partial S}{\partial Z_1}$$

It should be noted that, for a trapezoidal planar element, $\bar{\alpha}$ and $\bar{\beta}$ are constants and that, according to Eq. (B.1),

$$\bar{\delta} = (Z_1-Z) - \bar{\alpha}(X_1-X) - \bar{\beta}(Y_1-Y)$$

$$= (Z_{1c}-Z) - \bar{\alpha}(X_{1c}-X) - \bar{\beta}(Y_{1c}-Y) \tag{B.6}$$

Thus, Eq. (B.3) reduces to

$$\hat{\hat{I}}_D = -S\bar{\delta}\int_{Y_{1m}}^{Y_{1p}} dY_1 \int_{X_{1m}+d_m(Y_1-Y)}^{X_{1p}+d_p(Y_1-Y)} \frac{1}{R^3} dX_1 \tag{B.7}$$

with

$$R = \{(X_1-X)^2 + (Y_1-Y)^2 + [(\bar{\delta} + \bar{\alpha}(X_1-X) + \bar{\beta}(Y_1-Y)]^2\}^{1/2}$$

$$= \{[(1+\bar{\alpha}^2)^{1/2}(X_1-X) + \bar{\alpha}(\bar{\beta}(Y_1-Y)+\delta)]^2 + \delta^2/(1+\alpha^2)(1+\alpha^2+\beta^2) \quad \text{(B.8)}$$

$$+ [(1+\bar{\alpha}^2+\bar{\beta}^2)^{1/2}(Y_1-Y) + \beta\delta/(1+\bar{\alpha}^2+\bar{\beta}^2)^{1/2}]^2/(1+\alpha^2)\}^{1/2}$$

$$= \{\xi^2 + \eta^2 + \zeta^2\}^{1/2}$$

where

$$\hat{\xi} = (1+\bar{\alpha}^2)^{1/2}(X_1-X) + \bar{\alpha}[\bar{\beta}(Y_1-Y)+\delta]/(1+\bar{\alpha}^2)^{1/2}$$
$$\hat{\eta} = [(1+\bar{\alpha}^2+\bar{\beta}^2)^{1/2}(Y_1-Y) + \beta\delta/(1+\bar{\alpha}^2+\bar{\beta}^2)^{1/2}]/(1+\bar{\alpha}^2)^{1/2} \quad \text{(B.9)}$$
$$\hat{\zeta} = \delta/(1+\bar{\alpha}^2+\bar{\beta}^2)^{1/2}$$

Integrating Eq. (B.7), one obtains

$$\hat{\hat{I}}_D = \frac{-S\delta}{(1+\bar{\alpha}^2)^{1/2}} \int_{Y_{1m}}^{Y_{1p}} \left[\frac{\hat{\xi}_p}{\hat{\eta}^2+\hat{\zeta}^2} \cdot \frac{1}{(\hat{\xi}_p^2+\hat{\eta}^2+\hat{\zeta}^2)^{1/2}} - \frac{\hat{\xi}_m}{\hat{\eta}^2+\hat{\zeta}^2} \frac{1}{(\hat{\xi}_m^2+\hat{\eta}^2+\hat{\zeta}^2)^{1/2}} \right] dY_1 \quad \text{(B.10)}$$

where

$$\hat{\xi}_p = (1+\bar{\alpha}^2)^{1/2}[X_{1p}-X+d_p(Y_1-Y)] + \bar{\alpha}[\bar{\beta}(Y_1-Y)+\delta]/[1+\bar{\alpha}^2]^{1/2} \quad \text{(B.11)}$$

$$= \xi_{op} + \xi_{1p}\hat{\eta}$$

and

$$\hat{\xi}_m = (1+\bar{\alpha}^2)^{1/2}[X_{1m}-X+d_m(Y_1-Y)] + \bar{\alpha}[\bar{\beta}(Y_1-Y)+\delta]/(1+\bar{\alpha}^2)^{1/2} \quad \text{(B.12)}$$

$$= \xi_{om} + \xi_{1m}\hat{\eta}$$

with

$$\xi_{op} = (1+\bar{\alpha}^2)^{1/2}\left[X_{1p} - X + (\bar{\alpha} - d_p\bar{\beta})\delta/(1+\bar{\alpha}^2+\bar{\beta}^2)\right]$$

$$\xi_{1p} = \left[\bar{\alpha}\bar{\beta} + (1+\bar{\alpha}^2)d_p\right] / \left[1+\bar{\alpha}^2+\bar{\beta}^2\right]^{1/2} \qquad \text{(B.13)}$$

$$\xi_{om} = (1+\bar{\alpha}^2)^{1/2}\left[X_{1m} - X + (\bar{\alpha} - d_m\bar{\beta})\delta/(1+\bar{\alpha}^2+\bar{\beta}^2)\right]$$

$$\xi_{1m} = \left[\bar{\alpha}\bar{\beta} + (1+\bar{\alpha}^2)d_m\right] / \left[1+\bar{\alpha}^2+\bar{\beta}^2\right]^{1/2}$$

Substituting Eqs. (B.11) and (B.12) into (B.10) for $\hat{\xi}_p$ and $\hat{\xi}_m$ and changing the variable of integration from Y_1 to η one obtains

$$\hat{\hat{I}}_b = \frac{-S\delta}{(1+\bar{\alpha}^2+\bar{\beta}^2)^{1/2}} \int_{\hat{\eta}_m}^{\hat{\eta}_p} \left[\frac{\xi_{op} + \xi_{1p}\hat{\eta}}{(\hat{\eta}^2+\hat{\zeta}^2)\left[(\xi_{op}+\xi_{1p}\hat{\eta})^2 + \hat{\eta}^2 + \hat{\zeta}^2\right]^{1/2}} - \frac{\xi_{om} + \xi_{1m}\hat{\eta}}{(\hat{\eta}^2+\hat{\zeta}^2)\left[(\xi_{om}+\xi_{1m}\hat{\eta})^2 + \hat{\eta}^2 + \hat{\zeta}^2\right]^{1/2}} \right] d\eta \qquad \text{(B.14)}$$

where

$$\hat{\eta}_m = \left[(1+\bar{\alpha}^2+\bar{\beta}^2)^{1/2}(Y_{1m}-Y) + \beta\delta/(1+\bar{\alpha}^2+\bar{\beta}^2)^{1/2}\right] / (1+\bar{\alpha}^2)^{1/2}$$

$$\hat{\eta}_p = \left[(1+\bar{\alpha}^2+\bar{\beta}^2)^{1/2}(Y_{1p}-Y) + \beta\delta/(1+\bar{\alpha}^2+\bar{\beta}^2)^{1/2}\right] / (1+\bar{\alpha}^2)^{1/2} \qquad \text{(B.15)}$$

Consider the indefinite integral

$$\hat{\hat{I}}_1 = \int \frac{\hat{\xi}_0 + \hat{\xi}_1\hat{\eta}}{\hat{\eta}^2+\hat{\zeta}^2} \left[(\hat{\xi}_0 + \hat{\xi}_1\hat{\eta})^2 + \hat{\eta}^2 + \hat{\zeta}^2\right]^{-1/2} d\eta \qquad \text{(B.16)}$$

This can be integrated by standard methods of integration; using the transformation

$$\hat{\eta} = -\frac{\hat{\xi}_0}{\hat{\xi}_1}\,\frac{\hat{t} - \hat{\zeta}^2\hat{\xi}_1^2/\hat{\xi}_0^2}{\hat{t}+1} \tag{B.17}$$

and integrating, yields

$$\hat{\hat{I}}_1 = \frac{1}{|\hat{\zeta}|}\tan^{-1}\left\{\frac{\hat{\xi}_0\hat{t}}{|\hat{\zeta}|}\left[\frac{1+\hat{\zeta}^2\hat{\xi}_1^2/\hat{\xi}_0^2}{\hat{t}^2+\hat{\zeta}^2\hat{\xi}_1^2/\hat{\xi}_0^2+\hat{\xi}_1^2(1+\hat{\zeta}^2\hat{\xi}_1^2/\hat{\xi}_0^2)}\right]\right\} \tag{B.18}$$

and, returning to the original variable, η,

$$\hat{\hat{I}}_1 = \frac{1}{|\hat{\zeta}|}\tan^{-1}\left\{\frac{\hat{\xi}_0}{|\hat{\zeta}|}\,\frac{\hat{\eta}-\hat{\xi}_1\hat{\zeta}^2/\hat{\xi}_0}{[(\hat{\xi}_0+\hat{\xi}_1\hat{\eta})^2+\hat{\eta}^2+\hat{\zeta}^2]^{1/2}}\right\} \tag{B.19}$$

Finally, by using Eq. (B.19), Eq. (B.14) reduces to

$$\hat{\hat{I}}_0 = -\frac{s\,\delta}{(1+\bar{\alpha}^2+\bar{\beta}^2)^{1/2}}\,\frac{\hat{\hat{I}}}{|\hat{\zeta}|} \tag{B.20}$$

with

$$\begin{aligned}\hat{\hat{I}} = {} & \tan^{-1}\left\{\frac{\hat{\xi}_{0p}}{|\hat{\zeta}|}\left(\hat{\eta}_p - \frac{\hat{\xi}_{1p}}{\hat{\xi}_{0p}}\hat{\zeta}^2\right)\frac{1}{\hat{\rho}_{pp}}\right\} \\ & - \tan^{-1}\left\{\frac{\hat{\xi}_{0p}}{|\hat{\zeta}|}\left(\hat{\eta}_m - \frac{\hat{\xi}_{1p}}{\hat{\xi}_{0p}}\hat{\zeta}^2\right)\frac{1}{\hat{\rho}_{pm}}\right\} \\ & - \tan^{-1}\left\{\frac{\hat{\xi}_{0p}}{|\hat{\zeta}|}\left(\hat{\eta}_p - \frac{\hat{\xi}_{1m}}{\hat{\xi}_{0m}}\hat{\zeta}^2\right)\frac{1}{\hat{\rho}_{mp}}\right\} \\ & + \tan^{-1}\left\{\frac{\hat{\xi}_{0p}}{|\hat{\zeta}|}\left(\hat{\eta}_m - \frac{\hat{\xi}_{1m}}{\hat{\xi}_{0m}}\hat{\zeta}^2\right)\frac{1}{\hat{\rho}_{mm}}\right\}\end{aligned} \tag{B.21}$$

where

$$\begin{aligned}
\hat{\rho}_{pp} &= [\hat{\xi}_{pp}^2 + \hat{\eta}_p^2 + \hat{\zeta}^2]^{1/2} \\
\hat{\rho}_{pm} &= [\hat{\xi}_{pm}^2 + \hat{\eta}_m^2 + \hat{\zeta}^2]^{1/2} \\
\hat{\rho}_{mp} &= [\hat{\xi}_{mp}^2 + \hat{\eta}_p^2 + \hat{\zeta}^2]^{1/2} \\
\hat{\rho}_{mm} &= [\hat{\xi}_{mm}^2 + \hat{\eta}_m^2 + \hat{\zeta}^2]^{1/2}
\end{aligned} \tag{B.22}$$

with

$$\begin{aligned}
\hat{\xi}_{pp} &= \hat{\xi}_{0p} + \hat{\xi}_{1p}\hat{\eta}_p \\
\hat{\xi}_{pm} &= \hat{\xi}_{0p} + \hat{\xi}_{1p}\hat{\eta}_m \\
\hat{\xi}_{mp} &= \hat{\xi}_{0m} + \hat{\xi}_{1m}\hat{\eta}_p \\
\hat{\xi}_{mm} &= \hat{\xi}_{0m} + \hat{\xi}_{1m}\hat{\eta}_m
\end{aligned} \tag{B.23}$$

B.3 Source Distribution

Finally, consider the integral of a source distribution of density $\frac{\partial S}{\partial X_1}/|\nabla_1 S|$ over a trapezoidal planar element, given by

$$\begin{aligned}
\hat{\hat{I}}_S &= \iint \frac{1}{R}\frac{\partial S}{\partial X_1}\frac{d\Sigma}{|\nabla_1 S|} \\
&= \frac{\partial S/\partial X_1}{|\partial S/\partial Z_1|}\int_{Y_{1m}}^{Y_{1p}} dY_1 \int_{X_{1m}+d_m(Y_1-Y)}^{X_{1p}+d_p(Y_1-Y)} \frac{1}{R}\,dX_1
\end{aligned} \tag{B.24}$$

where R is as shown in Eq. (B.8). Integrating Eq. (B.24) yields,

$$\begin{aligned}
\hat{\hat{I}}_S = \frac{-S\bar{\alpha}}{(1+\bar{\alpha}^2+\bar{\beta}^2)^{1/2}}\Bigg\{ &\int_{\hat{\eta}_m}^{\hat{\eta}_p} \ln\left[(\hat{\xi}_{0p}+\hat{\xi}_{1p}\hat{\eta}) + \sqrt{(\hat{\xi}_{0p}+\hat{\xi}_{1p}\eta)^2+\hat{\eta}^2+\hat{\zeta}^2}\,\right]d\eta \\
&- \int_{\hat{\eta}_m}^{\hat{\eta}_p} \ln\left[(\hat{\xi}_{0m}+\hat{\xi}_{1m}\hat{\eta}) + \sqrt{(\hat{\xi}_{0m}+\hat{\xi}_{1m}\hat{\eta})+\hat{\eta}^2+\hat{\zeta}^2}\,\right]d\eta\Bigg\}
\end{aligned} \tag{B.25}$$

where $\hat{\eta}_p$, $\hat{\eta}_m$, $\hat{\xi}_{0p}$, $\hat{\xi}_{1p}$, $\hat{\xi}_{0m}$, $\hat{\xi}_{1m}$, $\hat{\zeta}$ are defined in Eqs. (B.15),

(B.13) and (B.9). Consider the indefinite integral

$$\hat{\hat{I}}_2 = \int \ln(\hat{\xi}+\hat{\rho})\, d\hat{\eta} \tag{B.26}$$

with $\hat{\xi} = \hat{\xi}_0 + \hat{\xi}_1 \hat{\eta}$. Integrating by parts yields (note that $\partial\hat{\xi}/\partial\hat{\eta} = \hat{\xi}_1$)

$$\begin{aligned} \hat{\hat{I}}_2 &= \hat{\eta}\ln(\hat{\xi}+\hat{\rho}) - \int \hat{\eta}\, \frac{1}{\hat{\xi}+\hat{\rho}} \left(\hat{\xi}_1 + \frac{\hat{\xi}_1\hat{\xi}+\hat{\eta}}{\hat{\rho}}\right) d\hat{\eta} \\ &= \hat{\eta}\ln(\hat{\xi}+\hat{\rho}) - \int \left(\hat{\xi}_1\hat{\eta} + \frac{\hat{\eta}^2}{\hat{\xi}+\hat{\rho}}\right)\frac{1}{\hat{\rho}}\, d\hat{\eta} \end{aligned} \tag{B.27}$$

Note that

$$\begin{aligned} \frac{\hat{\eta}^2}{\hat{\xi}+\hat{\rho}}\,\frac{1}{\hat{\rho}} &= \frac{\hat{\eta}^2}{\hat{\xi}^2-\hat{\rho}^2}\,\frac{\hat{\xi}-\hat{\rho}}{\hat{\rho}} = -\frac{\hat{\eta}^2}{\hat{\eta}^2+\hat{\zeta}^2}\left(\frac{\hat{\xi}}{\hat{\rho}}-1\right) \\ &= -\frac{\hat{\eta}^2}{\hat{\eta}^2+\hat{\zeta}^2}\,\frac{\hat{\xi}}{\hat{\rho}} + \frac{\hat{\eta}^2}{\hat{\eta}^2+\hat{\zeta}^2} = -\frac{\hat{\xi}}{\hat{\rho}} + \frac{\hat{\xi}^2}{\hat{\eta}^2+\hat{\xi}^2}\,\frac{\hat{\xi}}{\hat{\rho}} + \frac{\hat{\eta}^2}{\hat{\eta}^2+\hat{\zeta}^2} \end{aligned} \tag{B.28}$$

Combining Eqs. B.27 and B.28 yields (note that $\hat{\xi}_1\hat{\eta} - \hat{\xi} = -\hat{\xi}_0$)

$$\hat{\hat{I}}_2 = \hat{\eta}\ln(\hat{\xi}+\hat{\rho}) + \hat{\xi}_0 \int \frac{1}{\hat{\rho}}\, d\hat{\eta} - \hat{\zeta}^2 \int \frac{\hat{\xi}}{\hat{\eta}^2+\hat{\zeta}^2}\,\frac{1}{\hat{\rho}}\, d\hat{\eta} - \int \frac{\hat{\eta}^2}{\hat{\eta}^2+\hat{\zeta}^2}\, d\hat{\eta} \tag{B.29}$$

Note that

$$\begin{aligned} \int \frac{1}{\hat{\rho}}\, d\hat{\eta} &= \int \left[(\hat{\xi}_0 + \hat{\xi}_1\eta)^2 + \hat{\eta}^2 + \hat{\zeta}^2\right]^{-1/2} d\hat{\eta} \\ &= \frac{1}{\sqrt{1+\hat{\xi}_1^2}} \ln\left(\hat{\eta} + \frac{\hat{\xi}_0\hat{\xi}_1}{1+\hat{\xi}_1^2} + \frac{\rho}{\sqrt{1+\hat{\xi}_1^2}}\right) \end{aligned} \tag{B.30}$$

Combining Eqs. (B.25), (B.29) and (B.30) yields

$$\hat{\hat{I}}_S = \frac{-5\bar{\alpha}}{\sqrt{1+\bar{\alpha}^2+\bar{\beta}^2}} \left\{ \left[\hat{\eta}_p \ln\left(\frac{\hat{\xi}_{pp} + \hat{\rho}_{pp}}{\hat{\xi}_{mp} + \hat{\rho}_{mp}} \right) - \hat{\eta}_m \ln\left(\frac{\hat{\xi}_{pm} + \hat{\rho}_{pm}}{\hat{\xi}_{mm} + \hat{\rho}_{mm}} \right) \right] \right.$$

$$+ \frac{\hat{\xi}_{op}}{\sqrt{1+\hat{\xi}_{1p}^2}} \ln\left(\frac{\hat{\eta}_p + \hat{\xi}_{op}\hat{\xi}_{1p}/(1+\hat{\xi}_{1p}^2) + \hat{\rho}_{pp}/\sqrt{1+\hat{\xi}_{1p}^2}}{\hat{\eta}_m + \hat{\xi}_{op}\hat{\xi}_{1p}/(1+\hat{\xi}_{1p}^2) + \hat{\rho}_{pm}/\sqrt{1+\hat{\xi}_{1p}^2}} \right)$$

$$- \frac{\hat{\xi}_{om}}{\sqrt{1+\hat{\xi}_{1m}^2}} \ln\left(\frac{\hat{\eta}_p + \hat{\xi}_{om}\hat{\xi}_{1m}/(1+\hat{\xi}_{1m}^2) + \hat{\rho}_{mp}/\sqrt{1+\hat{\xi}_{1m}^2}}{\hat{\eta}_m + \hat{\xi}_{om}\hat{\xi}_{1m}/(1+\hat{\xi}_{1m}^2) + \hat{\rho}_{mm}/\sqrt{1+\hat{\xi}_{1m}^2}} \right)$$

$$\left. - |\hat{\zeta}| \hat{\hat{I}} \right\} \qquad \text{(B.31)}$$

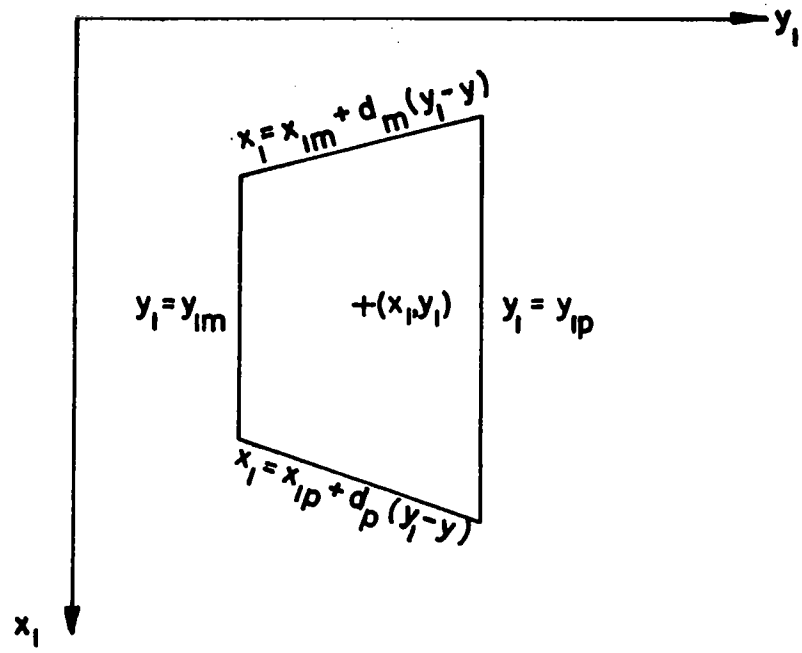

Fig. B.1 The projection of the trapezoidal element in the plane X_1, Y_1

APPENDIX C

GAUSSIAN QUADRATURE AROUND A SINGULAR POINT

C.1 Introduction

As mentioned in Subsection 4.3, the coefficients

$$C_{ki} = \iint_{\Sigma_i} \frac{\partial}{\partial N_1} \left(\frac{1}{2\pi R_k} \right) d\Sigma_i \qquad \text{C.1}$$

are evaluated by approximating the surface element Σ_i with its tangent plane at the centroid of the element. This value can eventually be corrected by adding the integral of difference between the original integrand and the (tangent-element) approximated integrand. This integration can be evaluated numerically by using standard Gaussian quadrature formulas. However, in the case of k = i (effect of the element on itself), the tangent plane contribution is equal to zero. Furthermore, the integrand becomes infinite when $R_k = 0$. Hence, a special integration scheme must be used. In this Appendix, an analysis of the type of singularity of the integrand of Eq. C.1 (when k = i) is given (Subsection C.2). Then a transformation that eliminates the singularity is presented (Subsection C.3).

C.2 Behavior of Doublets in the Neighborhood of Singularity

For simplicity, the analysis of the behavior of the doublet in the neighborhood R = 0 is performed with a frame of reference such that the origin is at the centroid of the element and the Z-axis is directed as the normal $\vec{n}$.

Then, the equation of the element can be written as

$$Z - F(X, Y) = 0 \qquad \text{C.2}$$

with Z = 0 for X = Y = 0 (Fig. C.1) and Eq. C.1 for K = i, reduces to

$$c_{kk} = -\iint_{\Sigma_k} \frac{h}{R^3}\, dX_1\, dY_1 \qquad \text{C.3}$$

where

$$h = -\frac{\partial F}{\partial X_1}(X_1 - X) - \frac{\partial F}{\partial Y_1}(Y_1 - Y) + (Z_1 - Z) \qquad \text{C.4}$$

is the distance along the normal N_1 of the origin from the point X_1, Y_1, Z_1 (Fig. C.2). If R goes to zero, the distance h goes also to zero.

$$h \sim cR^2 \qquad \text{C.5}$$

where $C = 1/\rho_c$ is the curvature of the cross section indicated in the figure (ρ_c is the radius of curvature). Thus, in a neighborhood of R = 0, Eq. C.3 reduces to

$$c_{kk} \cong -\iint \frac{C}{R}\, dX_1\, dY_1 \qquad \text{C.6}$$

It should be noted that C is the curvature of the cross section and thus C depends upon the angle Ψ of the cross section. Thus, in order to evaluate Eq. C.3, it is convenient to use polar coordinates since this eliminates the singularity 1/R as well as the sharp variations (in the plane X_1, Y_1) of the integrand, due to the dependence of C upon Ψ .

C.3 Integration Scheme

As shown above, the integration of Eq. C.1 (with k = i) in the neighborhood of the centroid of the element can be performed using standard quadrature techniques (Gaussian quadrature in particular) in polar coordinates. However, with these variables, the definition of domain of integration is not given by coordinate lines. Hence, a more suitable technique (fully correspondent to integration in polar coordinate) is described here.

As shown in Eqs. 4.29 and 4.30, the boundary of the element in the plane are given by

$$\bar{X}_c - \Delta\bar{X}/2 \leq \bar{X} \leq \bar{X}_c + \Delta\bar{X}/2$$
$$\bar{Y}_c - \Delta\bar{Y}/2 \leq \bar{Y} \leq \bar{Y}_c + \Delta\bar{Y}/2 \qquad \text{C.7}$$

Note that the use of

$$\xi = \bar{X}^2 \qquad \eta = [1 - (1-\bar{Y})^2] \qquad \text{C.8}$$

has the advantage of eliminating the square root singularity at the leading edge and the tip.* On the other hand, a singularity of the type R^{-1} in the plane X_1, Y_1 yields a singularity of the type , $\bar{R}^{-1}$ in the plane $\bar{X}$, $\bar{Y}$. Thus, the integral to be evaluated is of the type

---

*This singularity is due to the factor $|\nabla S|$ in $d\Sigma = \left|\frac{\nabla S}{\partial S/\partial Z}\right| dX dY$

$$C_{kk} = \iint_D \frac{f(\bar{X},\bar{Y})}{\sqrt{\bar{X}^2+\bar{Y}^2}}\, d\bar{X}\, d\bar{Y}$$

$$= \int_{\bar{Y}_c-\frac{\Delta\bar{Y}}{2}}^{\bar{Y}_c+\frac{\Delta\bar{Y}}{2}} d\bar{Y} \int_{\bar{X}_c-\frac{\Delta\bar{X}}{2}}^{\bar{X}_c+\frac{\Delta\bar{X}}{2}} \frac{f(\bar{X},\bar{Y})\, d\bar{X}}{\sqrt{\bar{X}^2+\bar{Y}^2}} \qquad \text{C.9}$$

where $f(\bar{X}, \bar{Y})$ is a finite but discontinuous function of $\bar{X}$, $\bar{Y}$ (the discontinuity being due to the "cross-section-curvature effect") although continuous in polar coordinate. In order to analyze Eq. C.7 it is convenient to separate the contributions of $D_1 + D_3$ and $D_2 + D_4$ (see Fig. C.3) as

$$C_{kk} = C'_{kk} + C''_{kk} \qquad \text{C.10}$$

with

$$C'_{kk} = \iint_{D_1+D_3} f(\bar{X},\bar{Y})/(\bar{X}^2+\bar{Y}^2)^{1/2}\, d\bar{X}\, d\bar{Y} \qquad \text{C.11}$$

$$C''_{kk} = \iint_{D_2+D_4} f(\bar{X},\bar{Y})/(\bar{X}^2+\bar{Y}^2)^{1/2}\, d\bar{X}\, d\bar{Y} \qquad \text{C.12}$$

Using the transformation

$$\bar{X} = \bar{X}_c + \frac{\Delta\bar{X}}{2}\, u \qquad -1 \le u \le 1$$
$$\bar{Y} = \bar{Y}_c + \frac{\Delta\bar{Y}}{2}\, uv \qquad -1 \le v \le 1 \qquad \text{C.13}$$

Equation C.11 reduces to

$$C'_{kk} = \frac{\Delta X \Delta Y}{4} \int_{-1}^{1}\int_{-1}^{1} \frac{f(u,v)\,|u|\, du\, dv}{\sqrt{(\bar{X}_c+\frac{\Delta\bar{X}}{2}u)^2+(\bar{Y}_c+\frac{\Delta\bar{Y}}{2}uv)^2}} = \frac{\Delta x \Delta Y}{4}\int_{-1}^{1}\int_{-1}^{1} \bar{f}(u,v)\, du dv \qquad \text{C.14}$$

Note that $\bar{f}(u, v)$ is a regular function of u and v since the factor $|u|$ compensates for the $(\bar{X}^2 + \bar{Y}^2)^{-1/2}$ singularity and

the "cross-section-curvature effect" disappears in the u, v plane (which is similar to polar-coordinate plane). Hence, Eq. C.14 can be evaluated by the Gaussian quadrature. Similar transformation can be used in Eq. C.12.

This procedure was used to evaluate not only the effect c_{kk} of the element on itself, but also for effect of an element on the opposite element. Similar technique is used also for the evaluation of

$$b_k = \sum_{i=1}^{N} b_{ki} = \sum_{i=1}^{N} \iint_{\Sigma_i} \varphi_n \frac{1}{R_k} d\Sigma_k \qquad \text{C.15}$$

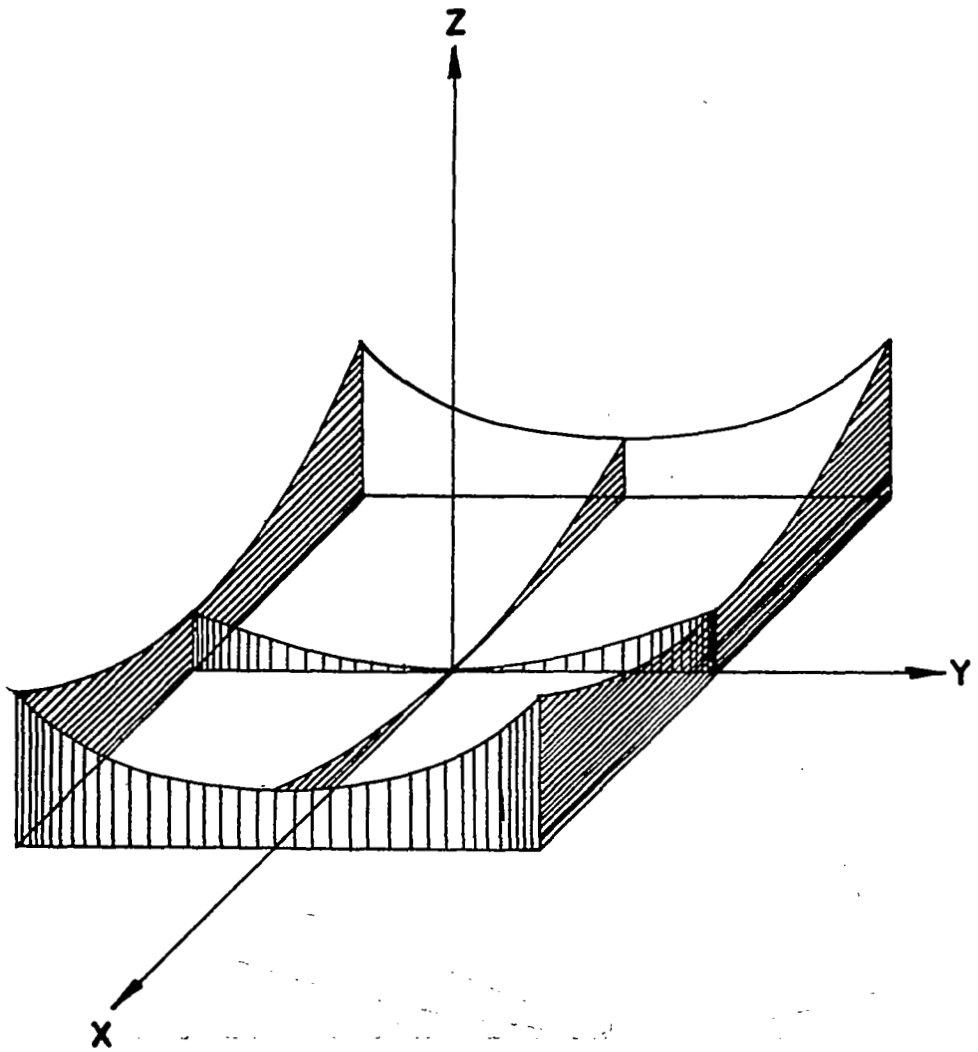

Fig. C.1 Surface Σ in neighborhood of R = 0

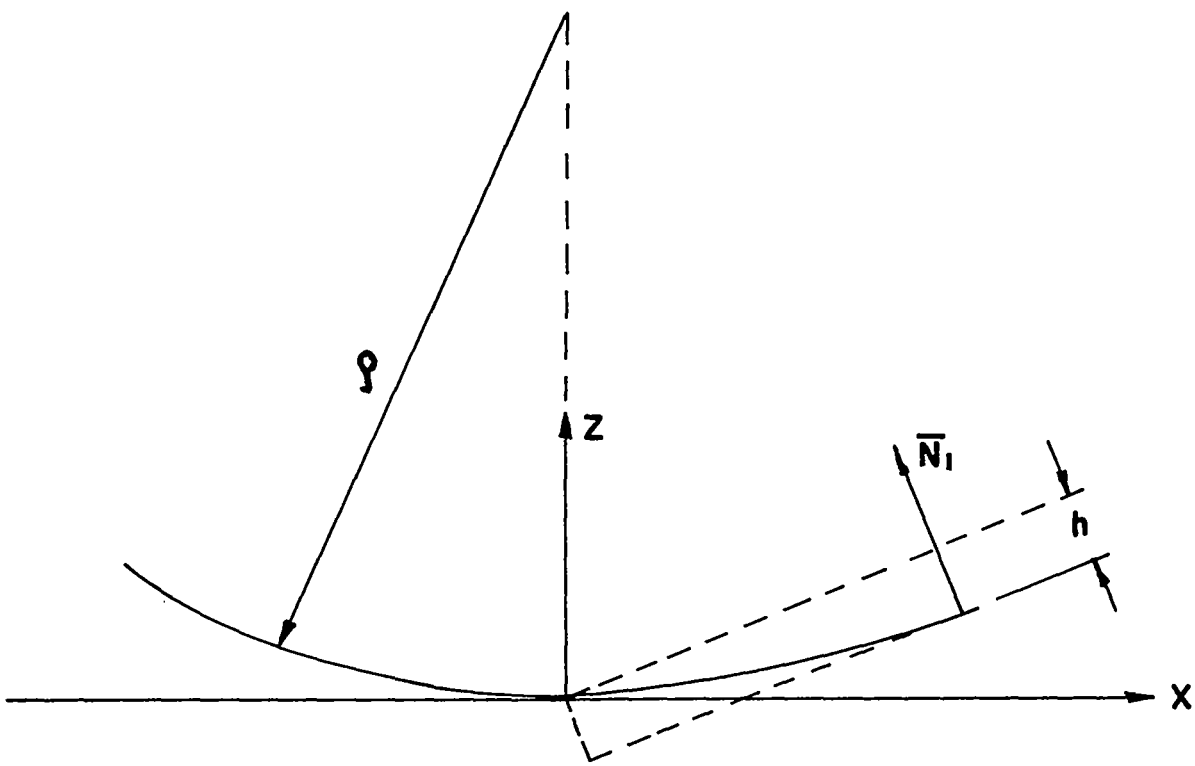

Fig. C.2 Curvature of cross section

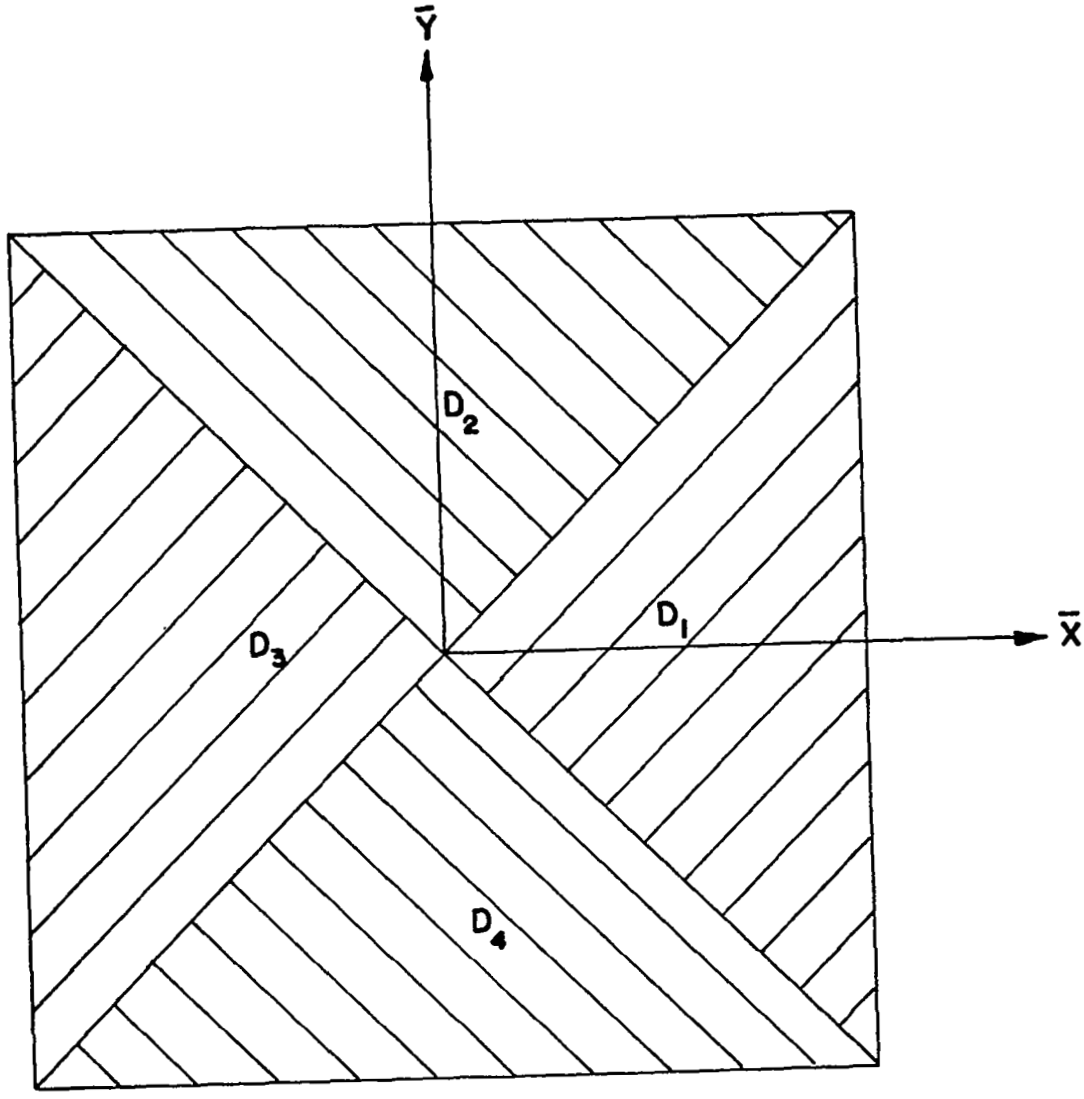

Fig. C.3 Domain of Integration